INTERNATIONAL JOURNAL FOR NUMERICAL METHODS IN FLUIDS
Int. J. Numer. Meth. Fluids 2009; **61**:1299–1330
Published online 6 February 2009 in Wiley InterScience (www.interscience.wiley.com). DOI: 10.1002/fld.1996

FEM simulation of turbulent flow in a turbine blade passage with dynamical fluid–structure interaction

Lixiang Zhang[1,*,†,‡], Yakun Guo[2,§] and Wenquan Wang[3,¶]

[1]*Department of Engineering Mechanics, Kunming University of Science and Technology, Kunming 650051, Yunnan, China*
[2]*School of Engineering, University of Aberdeen, Aberdeen AB24 3UE, U.K.*
[3]*Department of Engineering Mechanics, Kunming University of Science and Technology, Kunming 650051, Yunnan, China*

SUMMARY

Results are described from a combined mathematical modeling and numerical iteration schemes of flow and vibration. We consider the coupling numerical simulations of both turbulent flow and structure vibration induced by flow. The methodology used is based on the stabilized finite element formulations with time integration. A fully coupled model of flow and flow-induced structure vibration was established using a hydride generalized variational principle of fluid and solid dynamics. The spatial discretization of this coupling model is based on the finite element interpolating formulations for the fluid and solid structure, while the different time integration schemes are respectively used for fluid and solid structure to obtain a stabilized algorithm. For fluid and solid dynamics, Hughes' predictor multi-corrector algorithm and the Newmark method are monolithically used to realize a monolithic solution of the fully coupled model. The numerical convergence is ensured for small deformation vibrating problems of the structure by using different time steps for fluid and solid, respectively. The established model and the associated numerical methodology developed in the paper were then applied to simulate two different flows. The first one is the lid-driven square cavity flow with different Reynolds numbers of 1000, 400 and 100 and the second is the turbulent flows in a 3-D turbine blade passage with dynamical fluid–structure interaction. Good agreement between numerical simulations and measurements of pressure and vibration acceleration indicates that the finite element method formulations developed in this paper are appropriate to deal with the flow under investigation. Copyright © 2009 John Wiley & Sons, Ltd.

Received 17 August 2007; Revised 24 October 2008; Accepted 3 December 2008

*Correspondence to: Lixiang Zhang, Department of Engineering Mechanics, Kunming University of Science and Technology, 50 East Ring Road Kunming 650051, Yunnan, China.
†E-mail: zlxzcc@126.com, zlxzcc@yahoo.com.cn
‡Professor.
§Senior Lecturer.
¶PhD.

Contract/grant sponsor: National Natural Science Foundation of China (NSFC); contract/grant numbers: 50839003, 50579025

KEY WORDS: turbulent flows; fluid–structure interaction; flow-induced vibration; numerical simulations; finite element formulations; hydro-turbine

1. INTRODUCTION

A flow passage, consisting of 3-D hydro-turbine blades, is a complex geometry configuration. As high speed flow entering from the inlet interacts strongly with the blades to exchange its kinetic energy into machinery energy for generating electricity, a complicated evolution of the turbulent flow in the passage with high Reynolds number is produced in accompanying with such strong interaction between fluid and solid structure. The flow-induced vibration of the blade structure is called flow-induced vibrations [1, 2]. Such vibration interacts with flow near the wall surfaces as if there were many unsteady sources/sinks on the boundaries, thereby transferring the kinetic energy in/out of fluid. Such interacting mechanism between fluid and solid structure is called dynamical fluid–structure interaction (FSI).

Fluid interacting with flexible solid structure is frequently encountered in many industrial areas of civil, energy, mechanical, aerospace and biomechanical engineering. Modeling of the flow subjected to the interaction has been received much attention in recent years. The methodology of the numerical simulations has been extensively developed for modeling the turbulent flows. For example, the direct numerical simulation and the large eddy simulation (LES), being the most powerful tools to study turbulent flows, have been widely applied in past decade [3–16] to model the flow in which the Reynolds number is relatively low and the flow pattern is comparatively simple. With the rapid development of computing resources and techniques, study of complex turbulent flows with high Reynolds numbers becomes realistic. However, knowledge on the simulation of turbulent flows with dynamical FSI is still lacking as these attractive methods exclude the vibrations of solid structures. On one hand, the vibration of solid structure largely increases the difficulty of the generation of well body-fitted curvilinear meshes on a near-wall region, which likely leads to a failure of simulation due to the vibration intruding into the fluid cells. On the other hand, the incorporation of flow simulation and vibration analysis results in problem of numerical stability due to the significant difference in physical characteristics between fluid and solid. In previous studies, simulations of flow with moving and/or deforming boundaries are often performed using the arbitrary Lagrangian Eulerian formulation (ALE) [17–19], or the immersed boundary method (IBM) [20–24] to deal with kinetic efforts of the meshes due to moving boundary. Generally speaking, it is difficult to simultaneously include mutual dynamical influence between flow and flow-induced vibration. Comparing with ALE and IBM, the finite element formulations are probably a more appropriate and powerful tool to treat the dynamical FSI problems. Thus, simulation methodologies based on the finite element formulations were extensively studied and used successfully to model complicated FSI problems [25–37]. The motivation of this study, therefore, is to establish a fully coupled model and its solving methodology based on the finite element formulations of fluid and solid dynamics in order to effectively simulate flows with dynamical FSI and to explore conveniently temporal and spatial features of the turbulence in complex configuration.

Computing techniques used in the pervious studies for flow–vibration system may be classified as monolithic [38–42] and partitioned methods [43–46] for flow with moving boundary. In monolithic methods, vibration is closely related to flow as moving boundary at the same time level, whereas in partitioned methods, flow and vibration are separately solved in turn, which provides flexibility to choose different solvers for each of the modules. For example in Reference [43],

DOI: 10.1002/fld

a combination of LES for flow and finite element method (FEM) for flow-induced vibration was used to simulate the high Reynolds number turbulent flow in a strongly 3-D hydro-turbine blade passage with dynamical FSI. In fact, the finite element formulations have significant advantages in computing flow in a complex passage with dynamical FSI. Guruswamy and Byun [35, 36] computed respectively plate and shell structures in Eulerian and incompressible viscous flow fields using the finite element structures. They used a domain decomposition method, in which fluid and structure were solved in separate modules. Using the same method, Garica and Guruswamy [37] obtained the transonic aeroelastic response of a 3-D wing in incompressible viscous flow field. Teixeira and Awruch [34] improved the computational efficiency by reducing the internal degree of freedoms (DOFs) of the structure in the equation, namely, only DOFs corresponding to the interface were used in the solution. A significant achievement in the field of the finite element formulations for fluid and structure dynamics is the stabilized finite element formulations introduced by Hughes and co-workers [47, 48] and then further developed by Tezduyar [25, 28, 31, 32] and Tezduyar and Sathe [33]. The stabilized technique used in simulation was an adding term based on the streamline-upwind/Petrov–Galerkin and the pressure-stabilizing/Petrov–Galerkin formulations for compressible and incompressible flows, respectively. It is well known that a drawback of the approaches of the finite element formulations is that they produce an ill-conditioned coefficient matrix due to fluid mesh distortion generated by vibration/moving walls and distinguished substantial characteristics of fluid and solid structure. A straightforward approach to overcome this drawback is to develop an appropriate correction technique of meshes. Some algorithms based on pre-conditions are better solvers for treating the coupled formulations [33, 49, 50].

The focus of the present study is to establish a fully coupled model for flow and flow-induced vibration and its monolithically solving methodology based on the finite element formulations to simulate turbulent flows in a 3-D turbine blade passage with the dynamical FSI. To this end, a hydride generalized variational principle of fluid and solid dynamics based on a power dissipation balance in fluid–solid system under consideration is firstly developed to describe the dynamical interactions between fluid flow and flow-induced vibration. The Newmark method for solid structure and the predictor multi-corrector algorithm (PMCA) for fluid are respectively applied as the time integrations. An iteration scheme for both fluid and solid structure is integrated at the same time level to realize a monolithic solution of the fully coupled model. Two numerical examples have been performed to validate the model and the associated numerical methodology developed in this paper. The first numerical example is a benchmark problem of the lid-driven square cavity flow with the different Reynolds numbers of 1000, 400 and 100, and the second is the turbulent flow in a 3-D turbine blade passage cited from Reference [43]. Laboratory experiments were carried out to measure the vibration accelerations of the blade and the pressures at the surfaces of the blade using acceleration and Kulite LL-072-25A transducers mounted at the specified locations of the blade. Good agreement between numerical simulation and measurements was obtained, indicating that the numerical model developed can be applied to simulate the complex turbulent flow with the dynamic FSI.

2. HYBRID GENERALIZED VARIATIONAL PRINCIPLE OF FLUID AND SOLID DYNAMICS

The geometrical configuration of the flow passage under consideration in this study is shown in Figure 1, which is one blade passage taken from a hydro-turbine runner. The blade passage consists

DOI: 10.1002/fld

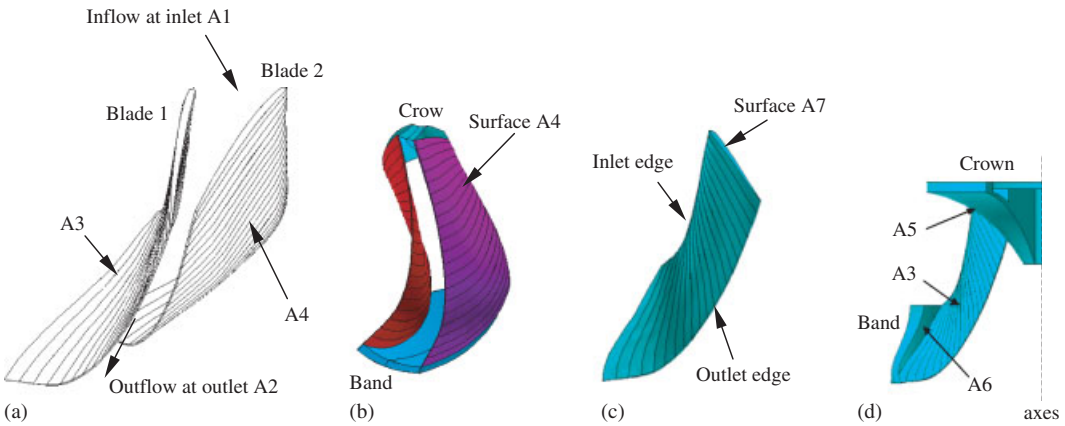

Figure 1. Components of hydro-turbine blade passage used in the present paper: (a) blade cascades; (b) blade passage; (c) blade; and (d) blade attached to crown and band.

of two blades, the crown and the band. The computational domains of fluid and solid structure are designated as Ω^{f} and Ω^{s}, respectively. The boundaries of the domains are $\Gamma^{\mathrm{f}}=\mathrm{A1}+\mathrm{A2}+\mathrm{A3}+\mathrm{A4}+A5+\mathrm{A6}$ for fluid and $\Gamma^{\mathrm{s}}=\mathrm{A3}+\mathrm{A4}+A5+\mathrm{A6}$ for solid structure, in which the inlet and outlet surfaces of fluid domain are defined as A1 and A2, the restricted surfaces of the blade attached to the crown and the band as A7 and A8 and the interfaces between fluid and solid structure as $\Gamma^{\mathrm{fs}}=\mathrm{A3}+\mathrm{A4}+A5+\mathrm{A6}$. We consider small magnitude vibration of solid structure excited by flow. The dynamical governing equations of the small magnitude vibration are stated as

$$\frac{\partial \dot{u}_i^{\mathrm{s}}}{\partial t}+c_{ij}\dot{u}_j^{\mathrm{s}}-\sigma_{ij,j}^{\mathrm{s}}-F_i^{\mathrm{s}}=0 \quad \text{in } \Omega^{\mathrm{s}} \tag{1}$$

$$p^{\mathrm{s}}=u_{k,k}^{\mathrm{s}} \quad \text{in } \Omega^{\mathrm{s}} \tag{2}$$

$$\sigma_{ij}^{\mathrm{s}}=\lambda^{\mathrm{s}}u_{k,k}^{\mathrm{s}}\delta_{ij}+v^{\mathrm{s}}(u_{i,j}^{\mathrm{s}}+u_{j,i}^{\mathrm{s}}) \quad \text{or} \quad \sigma_{ij}^{\mathrm{s}}=\lambda^{\mathrm{s}}p^{\mathrm{s}}\delta_{ij}+2v^{\mathrm{s}}\varepsilon_{ij}^{\mathrm{s}} \quad \text{in } \Omega^{\mathrm{s}} \tag{3}$$

$$\sigma_{ij}^{\mathrm{s}}n_j^{\mathrm{s}}+\sigma_{ij}^{\mathrm{f}}n_j^{\mathrm{f}}=0 \quad \text{on } \Gamma^{\mathrm{fs}} \tag{4}$$

For incompressible viscous fluid flowing through the blade passage, the governing equations of flow are

$$\frac{\partial \dot{u}_i^{\mathrm{f}}}{\partial t}+\dot{u}_j^{\mathrm{f}}\dot{u}_{i,j}^{\mathrm{f}}-\sigma_{ij,j}^{\mathrm{f}}-F_i^{\mathrm{f}}=0 \quad \text{in } \Omega^{\mathrm{f}} \tag{5}$$

$$\sigma_{ij}^{\mathrm{f}}=-p^{\mathrm{f}}\delta_{ij}+v^{\mathrm{f}}(\dot{u}_{i,j}^{\mathrm{f}}+\dot{u}_{j,i}^{\mathrm{f}}) \quad \text{or} \quad \sigma_{ij}^{\mathrm{f}}=-p^{\mathrm{f}}\delta_{ij}+2v^{\mathrm{f}}\dot{\varepsilon}_{ij}^{\mathrm{f}} \quad \text{in } \Omega^{\mathrm{f}} \tag{6}$$

$$\dot{u}_{k,k}^{\mathrm{f}}=0 \quad \text{in } \Omega^{\mathrm{f}} \tag{7}$$

$$\dot{u}_i^{\mathrm{f}}=\dot{u}_{0i}^{\mathrm{f}} \quad \text{on A1 and A2} \tag{8}$$

$$\dot{u}_i^{\mathrm{f}}-\dot{u}_i^{\mathrm{s}}=0 \quad \text{on } \Gamma^{\mathrm{fs}} \tag{9}$$

$$\sigma_{ij}^{\mathrm{f}}n_j^{\mathrm{f}}+\sigma_{ij}^{\mathrm{s}}n_j^{\mathrm{s}}=0 \quad \text{on } \Gamma^{\mathrm{fs}} \tag{10}$$

DOI: 10.1002/fld

where σ_{ij}^* is the stress tensor (divided by the mass density ρ^*, the superscript star indicates fluid for $*=f$ and structure for $*=s$, respectively), ε_{ij}^* the strain tensor, c_{ij} the viscous damping coefficient tensor of the solid structure (divided by the mass density ρ^{s}), δ_{ij} the Kronecker delta, F_i^* the body forces, p^{f} the fluid pressure (divided by the mass density ρ^{f}), p^{s} the bulk strain of the solid structure, $\lambda^{\mathrm{s}}=E\upsilon/(1+\upsilon)(1-2\upsilon)\rho^{\mathrm{s}}$ and $\nu^{\mathrm{s}}=E/2(1+\upsilon)\rho^{\mathrm{s}}$ the material constants of the solid structure, E and υ Young's modulus and Poisson's ratio, ν^{f} kinetic viscosity of fluid, $\dot{u}_i^*$ the velocity, n_j^* the outward normal unit vector of the boundary, the over-dot represents the derivatives with respect to time, $\dot{u}_{0i}^{\mathrm{f}}$ the known velocity conditions on the inlet ($\dot{u}_{0i}^{\mathrm{f}}=\dot{u}_{\mathrm{inlet}i}^{\mathrm{f}}$) and outlet ($\dot{u}_{0i}^{\mathrm{f}}=\dot{u}_{\mathrm{outlet}i}^{\mathrm{f}}$) surfaces A1 and A2, respectively, in which on the outlet surface A2 $\dot{u}_{0i}^{\mathrm{f}}=\dot{u}_{\mathrm{outlet}i}^{\mathrm{f}}$ is taken as the convective outflow condition.

The Bubnov–Galerkin method is used to deduce a system functional describing the interactions between fluid and solid structure. The functional variational form of the fluid–structure system is

$$\delta\hat{\Pi}^{\mathrm{fs}i}=\iiint_{\Omega^{\mathrm{f}}}\left(\frac{\partial\dot{u}_i^{\mathrm{f}}}{\partial t}+\dot{u}_j^{\mathrm{f}}\dot{u}_{i,j}^{\mathrm{f}}-\sigma_{ij,j}^{\mathrm{f}}-F_i^{\mathrm{f}}\right)G_i^{\mathrm{f}}\,\mathrm{d}\Omega+\iint_{\Gamma^{\mathrm{fs}}}(\sigma_{ij}^{\mathrm{f}}n_j^{\mathrm{f}}+\sigma_{ij}^{\mathrm{s}}n_j^{\mathrm{s}})H_i^{\mathrm{f}}\,\mathrm{d}A$$
$$+\iiint_{\Omega^{\mathrm{s}}}\left(\frac{\partial\dot{u}_i^{\mathrm{s}}}{\partial t}+c_{ij}\dot{u}_j^{\mathrm{s}}-\sigma_{ij,j}^{\mathrm{s}}-F_i^{\mathrm{s}}\right)G_i^{\mathrm{s}}\,\mathrm{d}\Omega+\iint_{\Gamma^{\mathrm{fs}}}(\sigma_{ij}^{\mathrm{s}}n_j^{\mathrm{s}}+\sigma_{ij}^{\mathrm{f}}n_j^{\mathrm{f}})H_i^{\mathrm{s}}\,\mathrm{d}A \tag{11}$$

where G_i^{f}, G_i^{s}, H_i^{f} and H_i^{s} are arbitrary weighted functions. Letting $G_i^{\mathrm{f}}=\delta\dot{u}_i^{\mathrm{f}}$, $G_i^{\mathrm{s}}=\delta\dot{u}_i^{\mathrm{s}}$, we obtain the formula below

$$\delta\hat{\Pi}^{\mathrm{fs}i}=\iiint_{\Omega^{\mathrm{f}}}\left[\frac{\partial\dot{u}_i^{\mathrm{f}}}{\partial t}\delta\dot{u}_i^{\mathrm{f}}+\dot{u}_j^{\mathrm{f}}\dot{u}_{i,j}^{\mathrm{f}}\delta\dot{u}_i^{\mathrm{f}}-F_i^{\mathrm{f}}\delta\dot{u}_i^{\mathrm{f}}+\frac{1}{2}\sigma_{ij}^{\mathrm{f}}\delta(\dot{u}_{i,j}^{\mathrm{f}}+\dot{u}_{j,i}^{\mathrm{f}})\right]\mathrm{d}\Omega$$
$$+\iiint_{\Omega^{\mathrm{s}}}\left[\frac{\partial\dot{u}_i^{\mathrm{s}}}{\partial t}\delta\dot{u}_i^{\mathrm{s}}+c_{ij}\dot{u}_j^{\mathrm{s}}\delta\dot{u}_i^{\mathrm{s}}-F_i^{\mathrm{s}}\delta\dot{u}_i^{\mathrm{s}}+\frac{1}{2}\sigma_{ij}^{\mathrm{s}}\delta(\dot{u}_{i,j}^{\mathrm{s}}+\dot{u}_{j,i}^{\mathrm{s}})\right]\mathrm{d}\Omega$$
$$+\iint_{\Gamma^{\mathrm{fs}}}\sigma_{ij}^{\mathrm{f}}n_j^{\mathrm{f}}(H_i^{\mathrm{f}}-\delta\dot{u}_i^{\mathrm{f}})\,\mathrm{d}A+\iint_{\Gamma^{\mathrm{fs}}}\sigma_{ij}^{\mathrm{s}}n_j^{\mathrm{s}}(H_i^{\mathrm{s}}-\delta\dot{u}_i^{\mathrm{s}})\,\mathrm{d}A$$
$$+\iint_{\Gamma^{\mathrm{fs}}}(\sigma_{ij}^{\mathrm{s}}n_j^{\mathrm{s}}H_i^{\mathrm{f}}+\sigma_{ij}^{\mathrm{f}}n_j^{\mathrm{f}}H_i^{\mathrm{s}})\,\mathrm{d}A \tag{12}$$

Provided that $H_i^{\mathrm{f}}=\delta\dot{u}_i^{\mathrm{f}}$, $H_i^{\mathrm{s}}=\delta\dot{u}_i^{\mathrm{s}}$, the above equation can be simplified as

$$\delta\hat{\Pi}_i^{\mathrm{fs}i}=\iiint_{\Omega^{\mathrm{f}}}\left[\left(\frac{\partial\dot{u}_i^{\mathrm{f}}}{\partial t}+\dot{u}_j^{\mathrm{f}}\dot{u}_{i,j}^{\mathrm{f}}-F_i^{\mathrm{f}}\right)\delta\dot{u}_i^{\mathrm{f}}+\frac{1}{2}\sigma_{ij}^{\mathrm{f}}\delta(\dot{u}_{i,j}^{\mathrm{f}}+\dot{u}_{j,i}^{\mathrm{f}})\right]\mathrm{d}\Omega$$
$$+\iiint_{\Omega^{\mathrm{s}}}\left[\left(\frac{\partial\dot{u}_i^{\mathrm{s}}}{\partial t}+c_{ij}\dot{u}_j^{\mathrm{s}}-F_i^{\mathrm{s}}\right)\delta\dot{u}_i^{\mathrm{s}}+\frac{1}{2}\sigma_{ij}^{\mathrm{s}}\delta(\dot{u}_{i,j}^{\mathrm{s}}+\dot{u}_{j,i}^{\mathrm{s}})\right]\mathrm{d}\Omega$$
$$+\iint_{\Gamma^{\mathrm{fs}}}(\sigma_{ij}^{\mathrm{s}}n_j^{\mathrm{s}}\delta\dot{u}_i^{\mathrm{f}}+\sigma_{ij}^{\mathrm{f}}n_j^{\mathrm{f}}\delta\dot{u}_i^{\mathrm{s}})\,\mathrm{d}A \tag{13}$$

DOI: 10.1002/fld

From Equations (3) and (6), $\delta(u^{\mathrm{s}}_{i,j}+u^{\mathrm{s}}_{j,i})$ and $\delta(\dot{u}^{\mathrm{f}}_{i,j}+\dot{u}^{\mathrm{f}}_{j,i})$ are expressed as

$$\delta(u^{\mathrm{s}}_{i,j}+u^{\mathrm{s}}_{j,i})=\frac{1}{v^{\mathrm{s}}}\delta\sigma^{\mathrm{s}}_{ij}-\frac{\lambda^{\mathrm{s}}}{v^{\mathrm{s}}}\delta p^{\mathrm{s}}\delta_{ij} \tag{14}$$

$$\delta(\dot{u}^{\mathrm{f}}_{i,j}+\dot{u}^{\mathrm{f}}_{j,i})=\frac{1}{v^{\mathrm{f}}}\delta\sigma^{\mathrm{f}}_{ij}+\frac{1}{v^{\mathrm{f}}}\delta p^{\mathrm{f}}\delta_{ij} \tag{15}$$

$$\sigma^{\mathrm{f}}_{ii}=-3p^{\mathrm{f}}+2v^{\mathrm{f}}\dot{u}^{\mathrm{f}}_{i,i}=-3p^{\mathrm{f}} \tag{16}$$

$$\sigma^{\mathrm{s}}_{ii}=3\lambda^{\mathrm{s}}p^{\mathrm{s}}+2v^{s}u^{\mathrm{s}}_{i,i}=(3\lambda^{\mathrm{s}}+2v^{\mathrm{s}})p^{\mathrm{s}} \tag{17}$$

Substituting Equations (14)–(17) into Equation (13) yields another formulation of the functional variation of the system

$$\begin{aligned}\delta\hat{\Pi}^{\mathrm{fs}i}_{i}=&\iiint_{\Omega^{\mathrm{f}}}\left(\frac{\partial\dot{u}^{\mathrm{f}}_{i}}{\partial t}+\dot{u}^{\mathrm{f}}_{j}\dot{u}^{\mathrm{f}}_{i,j}\right)\delta\dot{u}^{\mathrm{f}}_{i}\,\mathrm{d}\Omega+\iiint_{\Omega^{\mathrm{s}}}\frac{\partial\dot{u}^{\mathrm{s}}_{i}}{\partial t}\delta\dot{u}^{\mathrm{s}}_{i}\,\mathrm{d}\Omega+\iiint_{\Omega^{\mathrm{s}}}c_{ij}\dot{u}^{\mathrm{s}}_{j}\delta\dot{u}^{\mathrm{s}}_{i}\,\mathrm{d}\Omega\\&+\delta\iiint_{\Omega^{\mathrm{f}}}\frac{1}{4v^{\mathrm{f}}}(\sigma^{\mathrm{f}}_{kl}\sigma^{\mathrm{f}}_{kl}-3p^{\mathrm{f}}p^{\mathrm{f}})\,\mathrm{d}\Omega+\delta\iiint_{\Omega^{\mathrm{s}}}\frac{1}{4v^{\mathrm{s}}}[\sigma^{\mathrm{s}}_{kl}\sigma^{\mathrm{s}}_{kl}-\lambda^{\mathrm{s}}(3\lambda^{\mathrm{s}}+2v^{\mathrm{s}})p^{\mathrm{s}}p^{\mathrm{s}}]\,\mathrm{d}\Omega\\&-\delta\iiint_{\Omega^{\mathrm{f}}}F^{\mathrm{f}}_{i}\dot{u}^{\mathrm{f}}_{i}\,\mathrm{d}\Omega-\delta\iiint_{\Omega^{\mathrm{s}}}F^{\mathrm{s}}_{i}\dot{u}^{\mathrm{s}}_{i}\,\mathrm{d}\Omega+\iint_{\Gamma^{\mathrm{fs}}}(\sigma^{\mathrm{s}}_{ij}n^{\mathrm{s}}_{j})\delta\dot{u}^{\mathrm{f}}_{i}\,\mathrm{d}A\\&+\iint_{\Gamma^{\mathrm{fs}}}(\sigma^{\mathrm{f}}_{ij}n^{\mathrm{f}}_{j})\delta\dot{u}^{\mathrm{s}}_{i}\,\mathrm{d}A\end{aligned} \tag{18}$$

The first and second terms on the right-hand side of Equation (18) represent the total kinetic energy of fluid and solid per unit time, the third and fourth are the viscous dissipative energy, the fifth is the elastic deforming energy reserved in solid, the sixth and seventh indicate the work done by body forces and the final two terms are defined as mutual work done between fluid and solid structure due to interaction. Obviously, the functional $\hat{\Pi}^{\mathrm{fs}i}_{i}$ represents the dissipative power in the fluid–solid system; thus, it is called power functional of the system in the present paper.

As it is convenient to use $\dot{u}^{\mathrm{f}}_{i}$, p^{f} and u^{s}_{i} as unknowns of the system under consideration, $\sigma^{\mathrm{f}}_{kl}\sigma^{\mathrm{f}}_{kl}-3p^{\mathrm{f}}p^{\mathrm{f}}$ and $\sigma^{\mathrm{s}}_{kl}\sigma_{kl}-\lambda^{\mathrm{s}}(3\lambda^{\mathrm{s}}+2v^{\mathrm{s}})p^{\mathrm{s}}p^{\mathrm{s}}$ in Equation (18) are replaced using following formulas:

$$\sigma^{\mathrm{f}}_{ij}\sigma^{\mathrm{f}}_{ij}-3p^{\mathrm{f}}p^{\mathrm{f}}=2(v^{\mathrm{f}})^{2}(\dot{u}^{\mathrm{f}}_{i,j}+\dot{u}^{\mathrm{f}}_{j,i})\dot{u}^{\mathrm{f}}_{i,j} \tag{19}$$

$$\sigma^{\mathrm{s}}_{ij}\sigma_{ij}-\lambda^{\mathrm{s}}(3\lambda^{\mathrm{s}}+2v^{\mathrm{s}})p^{\mathrm{s}}p^{\mathrm{s}}=2(v^{\mathrm{s}})^{2}(u^{\mathrm{s}}_{i,j}+u^{\mathrm{s}}_{j,i})u^{\mathrm{s}}_{i,j} \tag{20}$$

Thus, Equation (18) is rewritten as

$$\begin{aligned}\delta\hat{\Pi}^{\mathrm{fs}i}_{i}=&\iiint_{\Omega^{\mathrm{f}}}\left(\frac{\partial\dot{u}^{\mathrm{f}}_{i}}{\partial t}+\dot{u}^{\mathrm{f}}_{j}\dot{u}^{\mathrm{f}}_{i,j}-F^{\mathrm{f}}_{i}\right)\delta\dot{u}^{\mathrm{f}}_{i}\,\mathrm{d}\Omega+\iiint_{\Omega^{\mathrm{s}}}\left(\frac{\partial\dot{u}^{\mathrm{s}}_{i}}{\partial t}+c_{ij}\dot{u}^{\mathrm{s}}_{j}-F^{\mathrm{s}}_{i}\right)\delta\dot{u}^{\mathrm{s}}_{i}\,\mathrm{d}\Omega\\&+\delta\iiint_{\Omega^{\mathrm{f}}}\frac{v^{\mathrm{f}}}{2}(\dot{u}^{\mathrm{f}}_{i,j}+\dot{u}^{\mathrm{f}}_{j,i})\dot{u}^{\mathrm{f}}_{i,j}\,\mathrm{d}\Omega+\delta\iiint_{\Omega^{\mathrm{s}}}\frac{v^{\mathrm{s}}}{2}(u^{\mathrm{s}}_{i,j}+u^{\mathrm{s}}_{j,i})u^{\mathrm{s}}_{i,j}\,\mathrm{d}\Omega\\&+\iint_{\Gamma^{\mathrm{fs}}}[\lambda^{\mathrm{s}}p^{\mathrm{s}}n^{\mathrm{s}}_{j}\delta_{ij}+v^{\mathrm{s}}(u^{\mathrm{s}}_{i,j}+u^{\mathrm{s}}_{j,i})n^{\mathrm{s}}_{j}]\delta\dot{u}^{\mathrm{f}}_{i}\,\mathrm{d}A\\&+\iint_{\Gamma^{\mathrm{fs}}}[-p^{\mathrm{f}}n^{\mathrm{f}}_{j}\delta_{ij}+v^{\mathrm{f}}(\dot{u}^{\mathrm{f}}_{i,j}+\dot{u}^{\mathrm{f}}_{j,i})n^{\mathrm{f}}_{j}]\delta\dot{u}^{\mathrm{s}}_{i}\,\mathrm{d}A\end{aligned} \tag{21}$$

DOI: 10.1002/fld

Three types of Lagrangian multipliers of γ, π_i and λ_i are employed to relax three restricted conditions, namely Equations (7), (8) and (9). A generalized variational principle based on fluid and solid mechanics is thus constructed as

$$\delta\Pi_i^{\mathrm{fs}i}=\delta\hat{\Pi}_i^{\mathrm{fs}i}+\delta\int\!\!\int\!\!\int_{\Omega^{\mathrm{f}}}\gamma\dot{u}^{\mathrm{f}}_{k,k}\,\mathrm{d}\Omega+\delta\int\!\!\int_{\mathrm{A1+A2}}\pi_i(\dot{u}_i^{\mathrm{f}}-\dot{u}_{0i}^{\mathrm{f}})\,\mathrm{d}A+\delta\int\!\!\int_{\Gamma^{\mathrm{fs}}}\lambda_i(\dot{u}_i^{\mathrm{f}}-\dot{u}_i^{\mathrm{s}})\,\mathrm{d}A \tag{22}$$

Expanding Equation (22) by using variational operation, the following formulation is obtained:

$$\begin{aligned}\delta\Pi_i^{\mathrm{fs}i}=&\int\!\!\int\!\!\int_{\Omega^{\mathrm{f}}}\left[\frac{\partial\dot{u}_i^{\mathrm{f}}}{\partial t}+\dot{u}_j^{\mathrm{f}}\dot{u}_{i,j}^{\mathrm{f}}-F_i^{\mathrm{f}}-\gamma_{,i}-\nu^{\mathrm{f}}(\dot{u}_{i,j}^{\mathrm{f}}+\dot{u}_{j,i}^{\mathrm{f}})_{,j}\right]\delta\dot{u}_i^{\mathrm{f}}\,\mathrm{d}\Omega+\int\!\!\int\!\!\int_{\Omega^{\mathrm{f}}}\delta\gamma\dot{u}_{k,k}^{\mathrm{f}}\,\mathrm{d}\Omega\\&+\int\!\!\int\!\!\int_{\Omega^{\mathrm{s}}}\left[\frac{\partial\dot{u}_i^{\mathrm{s}}}{\partial t}+c_{ij}\dot{u}_j^{\mathrm{s}}-F_i^{\mathrm{s}}-\lambda^{\mathrm{s}}p^{\mathrm{s}}{}_{,j}\delta_{ij}-\nu^{\mathrm{s}}(u_{i,j}^{\mathrm{s}}+u_{j,i}^{\mathrm{s}})_{,j}\right]\delta\dot{u}_i^{\mathrm{s}}\,\mathrm{d}\Omega\\&+\int\!\!\int_{\mathrm{A1+A2}}[\pi_i+\gamma n_j^{\mathrm{f}}\delta_{ij}+\nu^{\mathrm{f}}(\dot{u}_{i,j}^{\mathrm{f}}+\dot{u}_{j,i}^{\mathrm{f}})n_j^{\mathrm{f}}]\delta\dot{u}_i^{\mathrm{f}}\,\mathrm{d}A\\&+\int\!\!\int_{\Gamma^{\mathrm{fs}}}\{[\lambda_i+\gamma n_j^{\mathrm{f}}\delta_{ij}+\nu^{\mathrm{f}}(\dot{u}_{i,j}^{\mathrm{f}}+\dot{u}_{j,i}^{\mathrm{f}})n_j^{\mathrm{f}}]+[\lambda^{\mathrm{s}}p^{\mathrm{s}}\delta_{ij}n_j^{\mathrm{s}}+\nu^{\mathrm{s}}(u_{i,j}^{\mathrm{s}}+u_{j,i}^{\mathrm{s}})n_j^{\mathrm{s}}]\}\delta\dot{u}_i^{\mathrm{f}}\,\mathrm{d}A\\&+\int\!\!\int_{\Gamma^{\mathrm{fs}}}\{[-p^{\mathrm{f}}\delta_{ij}n_j^{\mathrm{f}}+\nu^{\mathrm{f}}(\dot{u}_{i,j}^{\mathrm{f}}+\dot{u}_{j,i}^{\mathrm{f}})n_j^{\mathrm{f}}]-\lambda_i+[\lambda^{\mathrm{s}}p^{\mathrm{s}}n_j^{\mathrm{s}}\delta_{ij}+\nu^{\mathrm{s}}(u_{i,j}^{\mathrm{s}}+u_{j,i}^{\mathrm{s}})n_j^{\mathrm{s}}]\}\delta\dot{u}_i^{\mathrm{s}}\,\mathrm{d}A\\&+\int\!\!\int_{\mathrm{A1+A2}}(\dot{u}_i^{\mathrm{f}}-\dot{u}_{0i}^{\mathrm{f}})\delta\pi_i\,\mathrm{d}A+\int\!\!\int_{\Gamma^{\mathrm{fs}}}(\dot{u}_i^{\mathrm{f}}-\dot{u}_i^{\mathrm{s}})\delta\lambda_i\,\mathrm{d}A\end{aligned} \tag{23}$$

Applying the variational stationary conditions, $\delta\Pi_i^{\mathrm{fs}i}=0$, we obtain the natural conditions of the variation for fluid as

$$\frac{\partial\dot{u}_i^{\mathrm{f}}}{\partial t}+\dot{u}_j^{\mathrm{f}}\dot{u}_{i,j}^{\mathrm{f}}-F_i^{\mathrm{f}}-\gamma_{,i}-\nu^{\mathrm{f}}(\dot{u}_{i,j}^{\mathrm{f}}+\dot{u}_{j,i}^{\mathrm{f}})_{,j}=0\quad\text{in }\Omega^{\mathrm{f}} \tag{24}$$

$$\dot{u}_{k,k}^{\mathrm{f}}=0\quad\text{in }\Omega^{\mathrm{f}} \tag{25}$$

$$\dot{u}_i^{\mathrm{f}}-\dot{u}_{0i}^{\mathrm{f}}=0\quad\text{on A1 and A2} \tag{26}$$

$$\dot{u}_i^{\mathrm{f}}-\dot{u}_i^{\mathrm{s}}=0\quad\text{on }\Gamma^{\mathrm{fs}} \tag{27}$$

$$\pi_i+\gamma n_j^{\mathrm{f}}\delta_{ij}+\nu^{\mathrm{f}}(\dot{u}_{i,j}^{\mathrm{f}}+\dot{u}_{j,i}^{\mathrm{f}})n_j^{\mathrm{f}}=0\quad\text{on A1 and A2} \tag{28}$$

$$\lambda_i+\gamma n_j^{\mathrm{f}}\delta_{ij}+\nu^{\mathrm{f}}(\dot{u}_{i,j}^{\mathrm{f}}+\dot{u}_{j,i}^{\mathrm{f}})n_j^{\mathrm{f}}+\lambda^{\mathrm{s}}p^{\mathrm{s}}\delta_{ij}n_j^{\mathrm{s}}+\nu^{\mathrm{s}}(u_{i,j}^{\mathrm{s}}+u_{j,i}^{\mathrm{s}})n_j^{\mathrm{s}}=0\quad\text{on }\Gamma^{\mathrm{fs}} \tag{29}$$

and for solid as

$$\frac{\partial\dot{u}_i^{\mathrm{s}}}{\partial t}+c_{ij}\dot{u}_j^{\mathrm{s}}-F_i^{\mathrm{s}}-\lambda^{\mathrm{s}}p^{\mathrm{s}}{}_{,j}\delta_{ij}-\nu^{\mathrm{s}}(u_{i,j}^{\mathrm{s}}+u_{j,i}^{\mathrm{s}})_{,j}=0\quad\text{in }\Omega^{\mathrm{s}} \tag{30}$$

$$-p^{\mathrm{f}}\delta_{ij}n_j^{\mathrm{f}}+\nu^{\mathrm{f}}(\dot{u}_{i,j}^{\mathrm{f}}+\dot{u}_{j,i}^{\mathrm{f}})n_j^{\mathrm{f}}-\lambda_i+\lambda^{\mathrm{s}}p^{s}n_j^{\mathrm{s}}\delta_{ij}+\nu^{\mathrm{s}}(u_{i,j}^{\mathrm{s}}+u_{j,i}^{\mathrm{s}})n_j^{\mathrm{s}}=0\quad\text{on }\Gamma^{\mathrm{fs}} \tag{31}$$

DOI: 10.1002/fld

The solutions of the Lagrangian multipliers are easily obtained as

$$\gamma = -p^{\mathrm{f}} \quad \text{in } \Omega^{\mathrm{f}} \tag{32}$$

$$\pi_i = -\sigma_{ij}^{\mathrm{f}} n_j^{\mathrm{f}} \quad \text{on A1 and A2} \tag{33}$$

$$\lambda_i = 0 \quad \text{on } \Gamma^{\mathrm{fs}} \tag{34}$$

where $\lambda_i = 0$ implies that the no-slip condition on the interface between fluid and solid structure is not stated as a natural condition of the hybrid generalized variational principle of the fluid–structure system due to unknown velocity on the interface. Therefore, instead of using Equation (27) as a natural condition, it is still used as a restricted condition, which leads to a partial hybrid generalized variational principle (PHGVP).

Substituting the solved Lagrangian multipliers of γ, π_i and λ_i into Equation (22) and applying the restricted condition of $\dot{u}_i^{\mathrm{f}} - \dot{u}_i^{\mathrm{s}} = 0$ yields the power functional variation of the coupling system based on PHGVP,

$$\delta\Pi_i^{\mathrm{fs}i} = \delta\hat{\Pi}_{i0}^{\mathrm{fs}i} - \delta\hat{\Pi}_{i1}^{\mathrm{fs}i} \tag{35}$$

The variational expansions of $\delta\hat{\Pi}_{i0}^{\mathrm{fs}i}$ and $\delta\hat{\Pi}_{i1}^{\mathrm{fs}i}$ are

$$\begin{aligned}\delta\hat{\Pi}_{i0}^{\mathrm{fs}i} = &\iiint_{\Omega^{\mathrm{f}}} \left[\left(\frac{\partial \dot{u}_i^{\mathrm{f}}}{\partial t} + \dot{u}_j^{\mathrm{f}} \dot{u}_{i,j}^{\mathrm{f}} - F_i^{\mathrm{f}} \right) \delta\dot{u}_i^{\mathrm{f}} + \sigma_{ij}^{\mathrm{f}} \delta\dot{\varepsilon}_{ij}^{\mathrm{f}} \right] \mathrm{d}\Omega \\ &+ \iiint_{\Omega^{\mathrm{s}}} \left[\left(\frac{\partial \dot{u}_i^{\mathrm{s}}}{\partial t} + c_{ij} \dot{u}_j^{\mathrm{s}} - F_i^{\mathrm{s}} \right) \delta\dot{u}_i^{\mathrm{s}} + \sigma_{ij}^{\mathrm{s}} \delta\dot{\varepsilon}_{ij}^{\mathrm{s}} \right] \mathrm{d}\Omega - \iiint_{\Omega^{\mathrm{f}}} (\delta p^{\mathrm{f}} \dot{u}_{k,k}^{\mathrm{f}} + p^{\mathrm{f}} \delta\dot{u}_{k,k}^{\mathrm{f}}) \, \mathrm{d}\Omega \end{aligned} \tag{36}$$

$$\begin{aligned}\delta\hat{\Pi}_{i1}^{\mathrm{fs}i} = &\iint_{\mathrm{A1+A2}} n_j^{\mathrm{f}} (\dot{u}_i^{\mathrm{f}} - \dot{u}_{0i}^{\mathrm{f}}) \delta\sigma_{ij}^{\mathrm{f}} \, \mathrm{d}A + \iint_{\mathrm{A1+A2}} \sigma_{ij}^{\mathrm{f}} n_j^{\mathrm{f}} \delta\dot{u}_i^{\mathrm{f}} \, \mathrm{d}A \\ &- \iint_{\Gamma^{\mathrm{fs}}} (\sigma_{ij}^{\mathrm{s}} n_j^{\mathrm{s}} \delta\dot{u}_i^{\mathrm{f}} + \sigma_{ij}^{\mathrm{f}} n_j^{\mathrm{f}} \delta\dot{u}_i^{\mathrm{s}}) \, \mathrm{d}A \end{aligned} \tag{37}$$

Equations (36) and (37) are the formulations of PHGVP for the coupling system under consideration.

3. FINITE ELEMENT FORMULATIONS ON PHGVP

In the present study, the finite element formulations are applied to create a flexible numerical scheme for both fluid and solid structure. To this end, the values of the variables $(\dot{u}_i^{\mathrm{f}}, p^{\mathrm{f}}, u_i^{\mathrm{s}})$ in element level are stated in an interpolation of the nodal values of an element, namely,

$$\dot{\mathbf{u}}^{\mathrm{f}}(x, y, z, t) = \mathbf{N}_e(x, y, z) \dot{\mathbf{u}}_e^{\mathrm{f}}(t) \tag{38}$$

$$\mathbf{p}^{\mathrm{f}}(x, y, z, t) = \hat{\mathbf{N}}_e(x, y, z) \mathbf{p}_e^{\mathrm{f}}(t) \tag{39}$$

DOI: 10.1002/fld

$$\mathbf{u}^{\mathrm{s}}(x,y,z,t)=\mathbf{N}_e(x,y,z)\mathbf{u}_e^{\mathrm{s}}(t) \tag{40}$$

$$\boldsymbol{\sigma}^{\mathrm{s}}=\mathbf{D}^{\mathrm{s}}\mathbf{L}\mathbf{u}^{\mathrm{s}}=\mathbf{D}^{\mathrm{s}}\mathbf{L}\mathbf{N}_e\mathbf{u}_e^{\mathrm{s}} \tag{41}$$

$$\boldsymbol{\sigma}^{\mathrm{f}}=\mathbf{D}^{\mathrm{p}}\mathbf{p}^{\mathrm{f}}+\mathbf{D}^{\mathrm{f}}\mathbf{L}\dot{\mathbf{u}}^{\mathrm{f}}=\mathbf{D}^{\mathrm{p}}\hat{\mathbf{N}}_e\mathbf{p}_e^{\mathrm{f}}+\mathbf{D}^{\mathrm{f}}\mathbf{L}\mathbf{N}_e\dot{\mathbf{u}}_e^{\mathrm{f}} \tag{42}$$

Thus, the finite element formulations based on PHGVP can be written in the global matrix notation as

$$\begin{aligned}
\delta\boldsymbol{\Pi}^{\mathrm{fs}i}=&\mathop{\mathrm{A}}_{e=1}^{\mathrm{EN}}\left\{\begin{array}{l}
\delta\dot{\mathbf{u}}_e^{\mathrm{fT}}\left\{\iiint_{\Omega_e^{\mathrm{f}}}\mathbf{N}_e^{\mathrm{T}}\mathbf{N}_e\ddot{\mathbf{u}}_e^{\mathrm{f}}+\mathbf{N}_e^{\mathrm{T}}\mathbf{N}_e\dot{\mathbf{u}}_e^{\mathrm{f}}(\partial\mathbf{N}_e)\dot{\mathbf{u}}_e^{\mathrm{f}}+(\mathbf{L}\mathbf{N}_e)^{\mathrm{T}}\mathbf{D}^{\mathrm{f}}(\mathbf{L}\mathbf{N}_e)\dot{\mathbf{u}}_e^{\mathrm{f}}-\mathbf{N}_e^{\mathrm{T}}\mathbf{N}_e\mathbf{F}_e^{\mathrm{f}}]\,\mathrm{d}\Omega\right.\\
\iiint_{\Omega_e^{\mathrm{f}}}[(\mathbf{L}\mathbf{N}_e)^{\mathrm{T}}\mathbf{D}^{\mathrm{p}}\hat{\mathbf{N}}_e\mathbf{p}_e^{\mathrm{f}}-\mathbf{N}_e^{\mathrm{T}}(\mathbf{L}^{\partial}\hat{\mathbf{N}}_e)\mathbf{p}_e^{\mathrm{f}}]\,\mathrm{d}\Omega+\iint_{\Gamma_e^{\mathrm{fs}}}\mathbf{N}_e^{\mathrm{T}}\mathbf{n}^{\mathrm{s}}\mathbf{D}^{\mathrm{s}}(\mathbf{L}\mathbf{N}_e)\mathbf{u}_e^{\mathrm{s}}\,\mathrm{d}A\\
\left.-\iint_{\mathrm{A1+A2}}[(\mathbf{n}^{\mathrm{f}}\mathbf{D}^{\mathrm{f}}\mathbf{L}\mathbf{N}_e)^{\mathrm{T}}\mathbf{N}_e(\dot{\mathbf{u}}_e^{\mathrm{f}}-\dot{\mathbf{u}}_{0e}^{\mathrm{f}})+(\mathbf{N}_e^{\mathrm{T}}\mathbf{n}^{\mathrm{f}}\mathbf{D}^{\mathrm{p}}\hat{\mathbf{N}}_e\mathbf{p}_e^{\mathrm{f}}+\mathbf{N}_e^{\mathrm{T}}\mathbf{n}^{\mathrm{f}}\mathbf{D}^{\mathrm{f}}(\mathbf{L}\mathbf{N}_e)\dot{\mathbf{u}}_e^{\mathrm{f}})]\,\mathrm{d}A\right\}
\end{array}\right\}\\
&-\mathop{\mathrm{A}}_{e=1}^{\mathrm{EN}}\left\{\delta\mathbf{p}_e^{\mathrm{fT}}\left[\iiint_{\Omega_e^{\mathrm{f}}}\hat{\mathbf{N}}_e^{\mathrm{T}}(\partial\mathbf{N}_e)\dot{\mathbf{u}}_e^{\mathrm{f}}\,\mathrm{d}\Omega+\iint_{\mathrm{A1+A2}}(\mathbf{n}^{\mathrm{f}}\mathbf{D}^{\mathrm{p}}\hat{\mathbf{N}}_e)^{\mathrm{T}}\mathbf{N}_e(\dot{\mathbf{u}}_e^{\mathrm{f}}-\dot{\mathbf{u}}_{0e}^{\mathrm{f}})\,\mathrm{d}A\right]\right\}\\
&+\mathop{\mathrm{A}}_{e=1}^{\mathrm{EN}}\left\{\begin{array}{l}
\delta\dot{\mathbf{u}}_e^{\mathrm{sT}}\left\{\iiint_{\Omega_e^{\mathrm{s}}}[\mathbf{N}_e^{\mathrm{T}}(\mathbf{N}_e\ddot{\mathbf{u}}_e^{\mathrm{s}}+\mathbf{C}_d\mathbf{N}_e\dot{\mathbf{u}}_e^{\mathrm{s}}-\mathbf{N}_e\mathbf{F}_e^{\mathrm{s}})+(\mathbf{L}\mathbf{N}_e)^{\mathrm{T}}\mathbf{D}^{\mathrm{s}}(\mathbf{L}\mathbf{N}_e)\mathbf{u}_e^{\mathrm{s}}]\,\mathrm{d}\Omega\right.\\
\left.+\iint_{\Gamma_e^{\mathrm{fs}}}\mathbf{N}_e^{\mathrm{T}}\mathbf{n}^{\mathrm{f}}[\mathbf{D}^{\mathrm{p}}\hat{\mathbf{N}}_e\mathbf{p}_e^{\mathrm{f}}+\mathbf{D}^{\mathrm{f}}(\mathbf{L}\mathbf{N}_e)\dot{\mathbf{u}}_e^{\mathrm{f}}]\,\mathrm{d}A\right\}
\end{array}\right\}
\end{aligned} \tag{43}$$

The corresponding vectors and matrices are defined as

$$\dot{\mathbf{u}}^{\mathrm{f}}(x,y,z,t)=[\dot{u}^{\mathrm{f}}\ \ \dot{v}^{\mathrm{f}}\ \ \dot{w}^{\mathrm{f}}]^{\mathrm{T}}$$

$$\mathbf{p}^{\mathrm{f}}(x,y,x,t)=[p^{\mathrm{f}}\ \ p^{\mathrm{f}}\ \ p^{\mathrm{f}}]^{\mathrm{T}}$$

$$\mathbf{u}^{\mathrm{s}}(x,y,z,t)=[u^{\mathrm{s}}\ \ v^{\mathrm{s}}\ \ w^{\mathrm{s}}]^{\mathrm{T}}$$

$$\dot{\mathbf{u}}_e^{\mathrm{f}}(t)=[\dot{u}_1^{\mathrm{f}}\ \ \dot{v}_1^{\mathrm{f}}\ \ \dot{w}_1^{\mathrm{f}}\ \ \ldots\ \ \dot{u}_i^{\mathrm{f}}\ \ \dot{v}_i^{\mathrm{f}}\ \ \dot{w}_i^{\mathrm{f}}\ \ \ldots\ \ \dot{u}_{\mathrm{NN}}^{\mathrm{f}}\ \ \dot{v}_{\mathrm{NN}}^{\mathrm{f}}\ \ \dot{w}_{\mathrm{NN}}^{\mathrm{f}}]_e^{\mathrm{T}}$$

$$\mathbf{p}_e^{\mathrm{f}}(t)=[p_1^{\mathrm{f}}\ \ p_1^{\mathrm{f}}\ \ p_1^{\mathrm{f}}\ \ \ldots\ \ p_i^{\mathrm{f}}\ \ p_i^{\mathrm{f}}\ \ p_i^{\mathrm{f}}\ \ \ldots\ \ p_{\mathrm{NN}}^{\mathrm{f}}\ \ p_{\mathrm{NN}}^{\mathrm{f}}\ \ p_{\mathrm{NN}}^{\mathrm{f}}]_e^{\mathrm{T}}$$

$$\mathbf{u}_e^{\mathrm{s}}(t)=[u_1^{\mathrm{s}}\ \ v_1^{\mathrm{s}}\ \ w_1^{\mathrm{s}}\ \ \ldots\ \ u_i^{\mathrm{s}}\ \ v_i^{\mathrm{s}}\ \ w_i^{\mathrm{s}}\ \ \ldots\ \ u_{\mathrm{NN}}^{\mathrm{s}}\ \ v_{\mathrm{NN}}^{\mathrm{s}}\ \ w_{\mathrm{NN}}^{\mathrm{s}}]_e^{\mathrm{T}}$$

$$\boldsymbol{\sigma}_e^{*}(x,y,z,t)=[\sigma_{xx}^{*}\ \ \sigma_{yy}^{*}\ \ \sigma_{zz}^{*}\ \ \sigma_{xy}^{*}\ \ \sigma_{yz}^{*}\ \ \sigma_{zx}^{*}]_e^{\mathrm{T}}$$

$$\mathbf{N}_e(x,y,z)=[\mathbf{I}N_1\ \ \ldots\ \ \mathbf{I}N_i\ \ \ldots\ \ \mathbf{I}N_{\mathrm{NN}}]_e$$

$$\hat{\mathbf{N}}_e(x,y,z)=[\mathbf{I}\hat{N}_1\ \ \ldots\ \ \mathbf{I}\hat{N}_i\ \ \ldots\ \ \mathbf{I}\hat{N}_{\mathrm{NN}}]_e$$

DOI: 10.1002/fld

$$\mathbf{D}^{\mathrm{f}}=\begin{bmatrix} 2v^{\mathrm{f}} & 0 & 0 & 0 & 0 & 0 \\ & 2v^{\mathrm{f}} & 0 & 0 & 0 & 0 \\ & & 2v^{\mathrm{f}} & 0 & 0 & 0 \\ & & & v^{\mathrm{f}} & 0 & 0 \\ & \text{sysmetry} & & & v^{\mathrm{f}} & 0 \\ & & & & & v^{\mathrm{f}} \end{bmatrix}$$

$$\mathbf{D}^{\mathrm{s}}=\begin{bmatrix} \lambda^{\mathrm{s}}+2v^{\mathrm{s}} & \lambda^{\mathrm{s}} & \lambda^{\mathrm{s}} & 0 & 0 & 0 \\ & \lambda^{\mathrm{s}}+2v^{\mathrm{s}} & \lambda^{\mathrm{s}} & 0 & 0 & 0 \\ & & \lambda^{\mathrm{s}}+2v^{\mathrm{s}} & 0 & 0 & 0 \\ & & & v^{\mathrm{s}} & 0 & 0 \\ & \text{sysmetry} & & & v^{\mathrm{s}} & 0 \\ & & & & & v^{\mathrm{s}} \end{bmatrix}$$

$$\mathbf{D}^{\mathrm{p}}=\begin{bmatrix} -1 & 0 & 0 \\ 0 & -1 & 0 \\ 0 & 0 & -1 \\ 0 & 0 & 0 \\ 0 & 0 & 0 \\ 0 & 0 & 0 \end{bmatrix}, \quad \mathbf{L}=\begin{bmatrix} \frac{\partial}{\partial x} & 0 & 0 \\ 0 & \frac{\partial}{\partial y} & 0 \\ 0 & 0 & \frac{\partial}{\partial z} \\ \frac{\partial}{\partial y} & \frac{\partial}{\partial x} & 0 \\ 0 & \frac{\partial}{\partial z} & \frac{\partial}{\partial y} \\ \frac{\partial}{\partial z} & 0 & \frac{\partial}{\partial x} \end{bmatrix}, \quad \mathbf{L}^{\partial}=\begin{bmatrix} \frac{\partial}{\partial x} & 0 & 0 \\ 0 & \frac{\partial}{\partial y} & 0 \\ 0 & 0 & \frac{\partial}{\partial z} \end{bmatrix}, \quad \partial=\begin{bmatrix} \frac{\partial}{\partial x} & \frac{\partial}{\partial y} & \frac{\partial}{\partial z} \end{bmatrix}$$

$$\mathbf{n}^{*}=\begin{bmatrix} n_x & 0 & 0 & n_y & 0 & n_z \\ 0 & n_x & 0 & n_y & n_z & 0 \\ 0 & 0 & n_x & 0 & n_y & n_z \end{bmatrix}$$

where $\mathbf{N}_e$ and $\hat{\mathbf{N}}_e$ are the element shape function matrices for the moving variables (flow velocity and displacement) and fluid pressure, respectively, $\mathbf{I}$ is a 3×3 identical matrix, $\mathrm{A}_{e=1}^{\mathrm{EN}}$ represents the finite element assembly operator, NN and EN denote the number of the element nodes and elements in the corresponding domain, superscript T stands for a transposed matrix and subscript e for the eth element in the discretized domain. Using the restricted conditions $\dot{u}_i^{\mathrm{f}}-\dot{u}_i^{\mathrm{s}}=0$ on the

DOI: 10.1002/fld

interface Γ^{fs} and the variational stationary conditions, $\delta\Pi_i^{\mathrm{fs}i}=0$, the finite element formulations of the fully coupled system under consideration are stated as

$$\begin{aligned}
&\mathop{\mathrm{A}}_{e=1}^{\mathrm{EN}}\left\{\iiint_{\Omega_e^{\mathrm{f}}}[\mathbf{N}_e^{\mathrm{T}}\mathbf{N}_e\ddot{\mathbf{u}}_{\mathbf{e}}^{\mathrm{f}}+\mathbf{N}_e^{\mathrm{T}}\mathbf{N}_e\dot{\mathbf{u}}_e^{\mathrm{f}}\partial\mathbf{N}_e\dot{\mathbf{u}}_e^{\mathrm{f}}+(\mathbf{L}\mathbf{N}_e)^{\mathrm{T}}\mathbf{D}^{\mathrm{f}}(\mathbf{L}\mathbf{N}_e)\dot{\mathbf{u}}_e^{\mathrm{f}}-\mathbf{N}_e^{\mathrm{T}}\mathbf{N}_e\mathbf{F}_e^{\mathrm{f}}]\,\mathrm{d}\Omega\right\}\\
&+\mathop{\mathrm{A}}_{e=1}^{\mathrm{EN}}\left\{\iiint_{\Omega_e^{\mathrm{f}}}[(\mathbf{L}\mathbf{N}_e)^{\mathrm{T}}\mathbf{D}^{\mathrm{p}}\hat{\mathbf{N}}_e\mathbf{p}_e^{\mathrm{f}}-\mathbf{N}_e^{\mathrm{T}}(\mathbf{L}^{\partial}\hat{\mathbf{N}}_e)\mathbf{p}_e^{\mathrm{f}}]\,\mathrm{d}\Omega\right\}+\mathop{\mathrm{A}}_{e=1}^{\mathrm{EN}}\left\{\iint_{\Gamma_e^{\mathrm{fs}}}\mathbf{N}_e^{\mathrm{T}}\mathbf{n}^{\mathrm{s}}\mathbf{D}^{\mathrm{s}}(\mathbf{L}\mathbf{N}_e)\mathbf{u}_e^{\mathrm{s}}\,\mathrm{d}A\right\}\\
&-\mathop{\mathrm{A}}_{e=1}^{\mathrm{EN}}\left\{\iint_{\mathrm{A1+A2}}[\mathbf{N}_e^{\mathrm{T}}\mathbf{n}^{\mathrm{f}}\mathbf{D}^{\mathrm{p}}\hat{\mathbf{N}}_e\mathbf{p}_e^{\mathrm{f}}+\mathbf{N}_e^{\mathrm{T}}\mathbf{n}^{\mathrm{f}}\mathbf{D}^{\mathrm{f}}(\mathbf{L}\mathbf{N}_e)\dot{\mathbf{u}}_e^{\mathrm{f}}]\,\mathrm{d}A\right\}=0
\end{aligned}\tag{44}$$

$$\mathop{\mathrm{A}}_{e=1}^{\mathrm{EN}}\left\{\iiint_{\Omega_e^{\mathrm{f}}}\hat{\mathbf{N}}_e^{\mathrm{T}}(\partial\mathbf{N}_e)\dot{\mathbf{u}}_e^{\mathrm{f}}\,\mathrm{d}\Omega\right\}=0\tag{45}$$

$$\begin{aligned}
&\mathop{\mathrm{A}}_{e=1}^{\mathrm{EN}}\left\{\iiint_{\Omega_e^{\mathrm{s}}}[\mathbf{N}_e^{\mathrm{T}}\mathbf{N}_e\ddot{\mathbf{u}}_{\mathbf{e}}^{\mathrm{s}}+\mathbf{N}_e^{\mathrm{T}}\mathbf{C}_d\mathbf{N}_e\dot{\mathbf{u}}_e^{\mathrm{s}}-\mathbf{N}_e^{\mathrm{T}}\mathbf{N}_e\mathbf{F}_e^{\mathrm{s}}+(\mathbf{L}\mathbf{N}_e)^{\mathrm{T}}\mathbf{D}^{\mathrm{s}}(\mathbf{L}\mathbf{N}_e)\mathbf{u}_e^{\mathrm{s}}]\,\mathrm{d}\Omega\right\}\\
&+\mathop{\mathrm{A}}_{e=1}^{\mathrm{EN}}\left\{\iint_{\Gamma_e^{\mathrm{fs}}}[\mathbf{N}_e^{\mathrm{T}}\mathbf{n}^{\mathrm{f}}\mathbf{D}^{\mathrm{p}}\hat{\mathbf{N}}_e\mathbf{p}_e^{\mathrm{f}}+\mathbf{N}_e^{\mathrm{T}}\mathbf{n}^{\mathrm{f}}\mathbf{D}^{\mathrm{f}}(\mathbf{L}\mathbf{N}_e)\dot{\mathbf{u}}_e^{\mathrm{f}}]\,\mathrm{d}A\right\}=0
\end{aligned}\tag{46}$$

Applying assembly operation to the element-level matrices, we can rewrite the above finite element formulations in global form as

$$\mathbf{M}^{\mathrm{f}}\dot{\mathbf{V}}^{\mathrm{f}}+\mathbf{C}^{\mathrm{f}}(\mathbf{V}^{\mathrm{f}})\mathbf{V}^{\mathrm{f}}+\mathbf{B}^{\mathrm{f}}\mathbf{P}^{\mathrm{f}}+\mathbf{K}^{\mathrm{s}}_{\Gamma^{\mathrm{fs}}}\mathbf{U}^{\mathrm{s}}=\mathbf{M}^{\mathrm{f}}\mathbf{F}^{\mathrm{f}}\tag{47}$$

$$\mathbf{C}^{\mathrm{c}}\mathbf{V}^{\mathrm{f}}=\mathbf{0}\tag{48}$$

$$\mathbf{M}^{\mathrm{s}}\ddot{\mathbf{U}}^{\mathrm{s}}+\mathbf{C}^{\mathrm{s}}\dot{\mathbf{U}}^{\mathrm{s}}+\mathbf{K}^{\mathrm{s}}\mathbf{U}^{\mathrm{s}}+\mathbf{B}^{\mathrm{f}}_{\Gamma^{\mathrm{fs}}}\mathbf{P}^{\mathrm{f}}+\mathbf{C}^{\mathrm{f}}_{\Gamma^{\mathrm{fs}}}\mathbf{V}^{\mathrm{f}}=\mathbf{M}^{\mathrm{s}}\mathbf{F}^{\mathrm{s}}\tag{49}$$

The above Equations (47)–(49) are subjected to the restricted condition on the interfaces Γ^{fs}

$$\mathbf{V}^{\mathrm{f}}_{\Gamma^{\mathrm{fs}}}-\dot{\mathbf{U}}^{\mathrm{s}}_{\Gamma^{\mathrm{fs}}}=0\tag{50}$$

where the global matrices and the nodal vectors are defined as

$$\mathbf{V}^{\mathrm{f}}=\begin{Bmatrix}\mathbf{V}^{\mathrm{f}}_{\mathrm{I}}\\ \mathbf{V}^{\mathrm{f}}_{\Gamma^{\mathrm{fs}}}\\ \mathbf{V}^{\mathrm{f}}_{\mathrm{A1}}=\mathbf{V}^{\mathrm{f}}_{\mathrm{inlet}}\\ \mathbf{V}^{\mathrm{f}}_{\mathrm{A2}}=\mathbf{V}^{\mathrm{f}}_{\mathrm{outlet}}\end{Bmatrix}=\begin{Bmatrix}\mathbf{V}^{\mathrm{f}}_1\\ \mathbf{V}^{\mathrm{f}}_2\end{Bmatrix},\quad \mathbf{P}^{\mathrm{f}}=\begin{Bmatrix}\mathbf{P}^{\mathrm{f}}_{\mathrm{I}}\\ \mathbf{P}^{\mathrm{f}}_{\Gamma^{\mathrm{fs}}}\\ \mathbf{P}^{\mathrm{f}}_{\mathrm{A1}}\\ \mathbf{P}^{\mathrm{f}}_{\mathrm{A2}}\end{Bmatrix}=\begin{Bmatrix}\mathbf{P}^{\mathrm{f}}_1\\ \mathbf{P}^{\mathrm{f}}_2\end{Bmatrix},\quad \mathbf{U}^{\mathrm{s}}=\begin{Bmatrix}\mathbf{U}^{\mathrm{s}}_{\mathrm{I}}\\ \mathbf{U}^{\mathrm{s}}_{\Gamma^{\mathrm{fs}}}\\ \mathbf{U}^{\mathrm{s}}_{\mathrm{A7}}=\mathbf{0}\\ \mathbf{U}^{\mathrm{s}}_{\mathrm{A8}}=\mathbf{0}\end{Bmatrix}=\begin{Bmatrix}\mathbf{U}^{\mathrm{s}}_1\\ \mathbf{U}^{\mathrm{s}}_2\end{Bmatrix}$$

DOI: 10.1002/fld

$$\mathbf{M}^{\mathrm{f}}=\begin{bmatrix}\mathbf{M}^{\mathrm{f}}_{\mathrm{II}} & \mathbf{M}^{\mathrm{f}}_{\mathrm{I}\Gamma^{\mathrm{fs}}} & \mathbf{M}^{\mathrm{f}}_{\mathrm{IA1}} & \mathbf{M}^{\mathrm{f}}_{\mathrm{IA2}}\\ \mathbf{M}^{\mathrm{f}}_{\Gamma^{\mathrm{fs}}\mathrm{I}} & \mathbf{M}^{\mathrm{f}}_{\Gamma^{\mathrm{fs}}\Gamma^{\mathrm{fs}}} & \mathbf{M}^{\mathrm{f}}_{\Gamma^{\mathrm{fs}}\mathrm{A1}} & \mathbf{M}^{\mathrm{f}}_{\Gamma^{\mathrm{fs}}\mathrm{A2}}\\ \mathbf{M}^{\mathrm{f}}_{\mathrm{A1I}} & \mathbf{M}^{\mathrm{f}}_{\mathrm{A1}\Gamma^{\mathrm{fs}}} & \mathbf{M}^{\mathrm{f}}_{\mathrm{A1A1}} & \mathbf{0}\\ \mathbf{M}^{\mathrm{f}}_{\mathrm{A2I}} & \mathbf{M}^{\mathrm{f}}_{\mathrm{A2}\Gamma^{\mathrm{fs}}} & \mathbf{0} & \mathbf{M}^{\mathrm{f}}_{\mathrm{A2A2}}\end{bmatrix}=\begin{bmatrix}\mathbf{M}^{\mathrm{f}}_{11} & \mathbf{M}^{\mathrm{f}}_{12}\\ \mathbf{M}^{\mathrm{f}}_{21} & \mathbf{M}^{\mathrm{f}}_{22}\end{bmatrix}$$

$$\mathbf{C}^{\mathrm{f}}(\mathbf{V}^{\mathrm{f}})=\begin{bmatrix}\mathbf{C}^{\mathrm{f}}_{\mathrm{II}} & \mathbf{C}^{\mathrm{f}}_{\mathrm{I}\Gamma^{\mathrm{fs}}} & \mathbf{C}^{\mathrm{f}}_{\mathrm{IA1}} & \mathbf{C}^{\mathrm{f}}_{IA2}\\ \mathbf{C}^{\mathrm{f}}_{\Gamma^{\mathrm{fs}}\mathrm{I}} & \mathbf{C}^{\mathrm{f}}_{\Gamma^{\mathrm{fs}}\Gamma^{\mathrm{fs}}} & \mathbf{C}^{\mathrm{f}}_{\Gamma^{\mathrm{fs}}\mathrm{A1}} & \mathbf{C}^{\mathrm{f}}_{\Gamma^{\mathrm{fs}}\mathrm{A2}}\\ \mathbf{C}^{\mathrm{f}}_{\mathrm{A1I}} & \mathbf{C}^{\mathrm{f}}_{\mathrm{A1}\Gamma^{\mathrm{fs}}} & \mathbf{C}^{\mathrm{f}}_{\mathrm{A1A1}} & \mathbf{0}\\ \mathbf{C}^{\mathrm{f}}_{\mathrm{A2I}} & \mathbf{C}^{\mathrm{f}}_{\mathrm{A2}\Gamma^{\mathrm{fs}}} & \mathbf{0} & \mathbf{C}^{\mathrm{f}}_{\mathrm{A2A2}}\end{bmatrix}=\begin{bmatrix}\mathbf{C}^{\mathrm{f}}_{11}(\mathbf{V}^{\mathrm{f}}) & \mathbf{C}^{\mathrm{f}}_{12}(\mathbf{V}^{\mathrm{f}})\\ \mathbf{C}^{\mathrm{f}}_{21}(\mathbf{V}^{\mathrm{f}}) & \mathbf{C}^{\mathrm{f}}_{22}\end{bmatrix}$$

$$\mathbf{B}^{\mathrm{f}}=\begin{bmatrix}\mathbf{B}^{\mathrm{f}}_{\mathrm{II}} & \mathbf{B}^{\mathrm{f}}_{\mathrm{I}\Gamma^{\mathrm{fs}}} & \mathbf{B}^{\mathrm{f}}_{\mathrm{IA1}} & \mathbf{B}^{\mathrm{f}}_{\mathrm{IA2}}\\ \mathbf{B}^{\mathrm{f}}_{\Gamma^{\mathrm{fs}}\mathrm{I}} & \mathbf{B}^{\mathrm{f}}_{\Gamma^{\mathrm{fs}}\Gamma^{\mathrm{fs}}} & \mathbf{B}^{\mathrm{f}}_{\Gamma^{\mathrm{fs}}\mathrm{A1}} & \mathbf{B}^{\mathrm{f}}_{\Gamma^{\mathrm{fs}}\mathrm{A2}}\\ \mathbf{B}^{\mathrm{f}}_{\mathrm{A1I}} & \mathbf{B}^{\mathrm{f}}_{\mathrm{A1}\Gamma^{\mathrm{fs}}} & \mathbf{B}^{\mathrm{f}}_{\mathrm{A1A1}} & \mathbf{0}\\ \mathbf{B}^{\mathrm{f}}_{\mathrm{A2I}} & \mathbf{B}^{\mathrm{f}}_{\mathrm{A2}\Gamma^{\mathrm{fs}}} & \mathbf{0} & \mathbf{B}^{\mathrm{f}}_{\mathrm{A2A2}}\end{bmatrix}=\begin{bmatrix}\mathbf{B}^{\mathrm{f}}_{11} & \mathbf{B}^{\mathrm{f}}_{12}\\ \mathbf{B}^{\mathrm{f}}_{21} & \mathbf{B}^{\mathrm{f}}_{22}\end{bmatrix}$$

$$\mathbf{C}^{\mathrm{c}}=\begin{bmatrix}\mathbf{C}^{\mathrm{c}}_{\mathrm{II}} & \mathbf{C}^{\mathrm{c}}_{\mathrm{I}\Gamma^{\mathrm{fs}}} & \mathbf{C}^{\mathrm{c}}_{\mathrm{IA1}} & \mathbf{C}^{\mathrm{c}}_{\mathrm{IA2}}\\ \mathbf{C}^{\mathrm{c}}_{\Gamma^{\mathrm{fs}}\mathrm{I}} & \mathbf{C}^{\mathrm{c}}_{\Gamma^{\mathrm{fs}}\Gamma^{\mathrm{fs}}} & \mathbf{C}^{\mathrm{c}}_{\Gamma^{\mathrm{fs}}\mathrm{A1}} & \mathbf{C}^{\mathrm{c}}_{\Gamma^{\mathrm{fs}}\mathrm{A2}}\\ \mathbf{C}^{\mathrm{c}}_{\mathrm{A1I}} & \mathbf{C}^{\mathrm{c}}_{\mathrm{A1}\Gamma^{\mathrm{fs}}} & \mathbf{C}^{\mathrm{c}}_{\mathrm{A1A1}} & \mathbf{0}\\ \mathbf{C}^{\mathrm{c}}_{\mathrm{A2I}} & \mathbf{C}^{\mathrm{c}}_{\mathrm{A2}\Gamma^{\mathrm{fs}}} & \mathbf{0} & \mathbf{C}^{\mathrm{c}}_{\mathrm{A2A2}}\end{bmatrix}=\begin{bmatrix}\mathbf{C}^{\mathrm{c}}_{11} & \mathbf{C}^{\mathrm{c}}_{12}\\ \mathbf{C}^{\mathrm{c}}_{21} & \mathbf{C}^{\mathrm{c}}_{22}\end{bmatrix}$$

$$\mathbf{C}^{\mathrm{f}}_{\Gamma^{\mathrm{fs}}}=\begin{bmatrix}\mathbf{0} & \mathbf{0} & \mathbf{0} & \mathbf{0}\\ \mathbf{0} & \mathbf{C}^{\mathrm{f}}_{\Gamma^{\mathrm{fs}}\Gamma^{\mathrm{fs}}} & \mathbf{0} & \mathbf{0}\\ \mathbf{0} & \mathbf{0} & \mathbf{0} & \mathbf{0}\\ \mathbf{0} & \mathbf{0} & \mathbf{0} & \mathbf{0}\end{bmatrix}=\begin{bmatrix}\mathbf{C}^{\mathrm{f}}_{\Gamma^{\mathrm{fs}}11} & \mathbf{0}\\ \mathbf{0} & \mathbf{0}\end{bmatrix}$$

$$\mathbf{B}^{\mathrm{f}}_{\Gamma^{\mathrm{fs}}}=\begin{bmatrix}\mathbf{0} & \mathbf{0} & \mathbf{0} & \mathbf{0}\\ \mathbf{0} & \mathbf{B}^{\mathrm{f}}_{\Gamma^{\mathrm{fs}}\Gamma^{\mathrm{fs}}} & \mathbf{0} & \mathbf{0}\\ \mathbf{0} & \mathbf{0} & \mathbf{0} & \mathbf{0}\\ \mathbf{0} & \mathbf{0} & \mathbf{0} & \mathbf{0}\end{bmatrix}=\begin{bmatrix}\mathbf{B}^{\mathrm{f}}_{\Gamma^{\mathrm{fs}}11} & \mathbf{0}\\ \mathbf{0} & \mathbf{0}\end{bmatrix}$$

DOI: 10.1002/fld

$$\mathbf{M}^{\mathrm{s}}=\begin{bmatrix}\mathbf{M}^{\mathrm{s}}_{\mathrm{II}} & \mathbf{M}^{\mathrm{s}}_{\mathrm{I}\Gamma^{\mathrm{fs}}} & \mathbf{0} & \mathbf{0}\\ \mathbf{M}^{\mathrm{s}}_{\Gamma^{\mathrm{fs}}\mathrm{I}} & \mathbf{M}^{\mathrm{s}}_{\Gamma^{\mathrm{fs}}\Gamma^{\mathrm{fs}}} & \mathbf{0} & \mathbf{0}\\ \mathbf{0} & \mathbf{0} & \mathbf{M}^{\mathrm{s}}_{\mathrm{A7A7}} & \mathbf{0}\\ \mathbf{0} & \mathbf{0} & \mathbf{0} & \mathbf{M}^{\mathrm{s}}_{\mathrm{A8A8}}\end{bmatrix}=\begin{bmatrix}\mathbf{M}^{\mathrm{s}}_{11} & \mathbf{0}\\ \mathbf{0} & \mathbf{M}^{\mathrm{s}}_{22}\end{bmatrix}$$

$$\mathbf{C}^{\mathrm{s}}=\begin{bmatrix}\mathbf{C}^{\mathrm{s}}_{\mathrm{II}} & \mathbf{C}^{\mathrm{s}}_{\mathrm{I}\Gamma^{\mathrm{fs}}} & \mathbf{0} & \mathbf{0}\\ \mathbf{C}^{\mathrm{s}}_{\Gamma^{\mathrm{fs}}\mathrm{I}} & \mathbf{C}^{\mathrm{s}}_{\Gamma^{\mathrm{fs}}\Gamma^{\mathrm{fs}}} & \mathbf{0} & \mathbf{0}\\ \mathbf{0} & \mathbf{0} & \mathbf{C}^{\mathrm{s}}_{\mathrm{A7A7}} & \mathbf{0}\\ \mathbf{0} & \mathbf{0} & \mathbf{0} & \mathbf{C}^{\mathrm{s}}_{\mathrm{A8A8}}\end{bmatrix}=\begin{bmatrix}\mathbf{C}^{\mathrm{s}}_{11} & \mathbf{0}\\ \mathbf{0} & \mathbf{C}^{\mathrm{s}}_{22}\end{bmatrix}$$

$$\mathbf{K}^{\mathrm{s}}=\begin{bmatrix}\mathbf{K}^{\mathrm{s}}_{\mathrm{II}} & \mathbf{K}^{\mathrm{s}}_{\mathrm{I}\Gamma^{\mathrm{fs}}} & \mathbf{0} & \mathbf{0}\\ \mathbf{K}^{\mathrm{s}}_{\Gamma^{\mathrm{fs}}\mathrm{I}} & \mathbf{K}^{\mathrm{s}}_{\Gamma^{\mathrm{fs}}\Gamma^{\mathrm{fs}}} & \mathbf{0} & \mathbf{0}\\ \mathbf{0} & \mathbf{0} & \mathbf{K}^{\mathrm{s}}_{\mathrm{A7A7}} & \mathbf{0}\\ \mathbf{0} & \mathbf{0} & \mathbf{0} & \mathbf{K}^{\mathrm{s}}_{\mathrm{A8A8}}\end{bmatrix}=\begin{bmatrix}\mathbf{K}^{\mathrm{s}}_{11} & \mathbf{0}\\ \mathbf{0} & \mathbf{K}^{\mathrm{s}}_{22}\end{bmatrix}$$

$$\mathbf{K}^{\mathrm{s}}_{\Gamma^{\mathrm{fs}}}=\begin{bmatrix}\mathbf{0} & \mathbf{0} & \mathbf{0} & \mathbf{0}\\ \mathbf{0} & \mathbf{K}^{\mathrm{s}}_{\Gamma^{\mathrm{fs}}\Gamma^{\mathrm{fs}}} & \mathbf{0} & \mathbf{0}\\ \mathbf{0} & \mathbf{0} & \mathbf{0} & \mathbf{0}\\ \mathbf{0} & \mathbf{0} & \mathbf{0} & \mathbf{0}\end{bmatrix}=\begin{bmatrix}\mathbf{K}^{\mathrm{s}}_{\Gamma^{\mathrm{fs}}11} & \mathbf{0}\\ \mathbf{0} & \mathbf{0}\end{bmatrix}$$

where the index translation is given below and the configurations of the nodes are shown in Figure 2.

I	all interior nodes in fluid or solid domain
A1	all nodes on surface A1
A2	all nodes on surface A2
Γ^{fs}	all nodes on interface Γ^{fs}
A7	all nodes on surface A7
A8	all nodes on surface A8
1	block consisting of unknowns
2	block consisting of known boundary conditions (except pressure vector)

The global matrices corresponding to the element matrices are defined as

$$\mathbf{M}^{\mathrm{f}}=\mathop{\mathrm{A}}_{e=1}^{\mathrm{EN}}\mathbf{M}^{\mathrm{f}}_{e}=\mathop{\mathrm{A}}_{e=1}^{\mathrm{EN}}\int\!\!\int\!\!\int_{\Omega^{\mathrm{f}}_{e}}\mathbf{N}^{\mathrm{T}}_{e}\mathbf{N}_{e}\,\mathrm{d}\Omega$$

$$\mathbf{C}^{\mathrm{f}}(\mathbf{V}^{\mathrm{f}})=\mathop{\mathrm{A}}_{e=1}^{\mathrm{EN}}\mathbf{C}^{\mathrm{f}}_{e}(\dot{\mathbf{u}}^{\mathrm{f}}_{e})=\mathop{\mathrm{A}}_{e=1}^{\mathrm{EN}}\int\!\!\int\!\!\int_{\Omega^{\mathrm{f}}_{e}}[\mathbf{N}^{\mathrm{T}}_{e}\mathbf{N}_{e}\dot{\mathbf{u}}^{\mathrm{f}}_{e}(\partial\mathbf{N}_{e})+(\mathbf{L}\mathbf{N}_{e})^{\mathrm{T}}\mathbf{D}^{\mathrm{f}}(\mathbf{L}\mathbf{N}_{e})]\,\mathrm{d}\Omega$$

DOI: 10.1002/fld

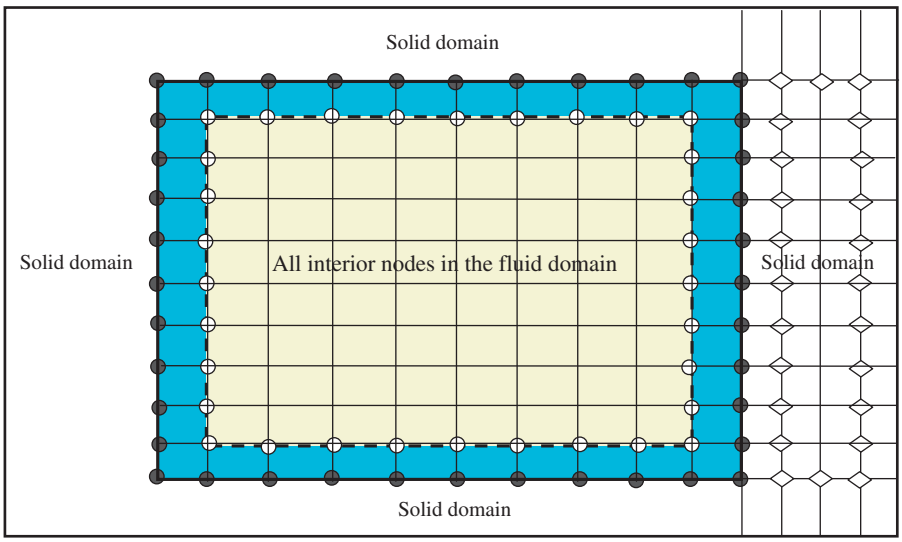

Figure 2. Nodal configurations in domains (the solid circles denote the shared nodes on the interface, the empty circles denote all interior nodes for the fluid domain and the empty diamonds denote all interior nodes for the solid domain).

$$\mathbf{C}^{\mathrm{f}}_{\Gamma^{\mathrm{fs}}\Gamma^{\mathrm{fs}}} = \mathop{\mathrm{A}}_{e=1}^{\mathrm{EN}} \mathbf{C}^{\mathrm{f}}_{\Gamma^{\mathrm{fs}}_e} = \mathop{\mathrm{A}}_{e=1}^{\mathrm{EN}} \int\int_{\Gamma^{\mathrm{fs}}_e} \mathbf{N}^{\mathrm{T}}_e \mathbf{n}^{\mathrm{f}} \mathbf{D}^{\mathrm{f}} (\mathbf{L}\mathbf{N}_e)\, \mathrm{d}A$$

$$\mathbf{C}^{\mathrm{f}}_{\mathrm{A1A1}} = \mathop{\mathrm{A}}_{e=1}^{\mathrm{EN}} \mathbf{C}^{\mathrm{f}}_{\mathrm{A1}e} = -\mathop{\mathrm{A}}_{e=1}^{\mathrm{EN}} \int\int_{\mathrm{A1}e} \mathbf{N}^{\mathrm{T}}_e \mathbf{n}^{\mathrm{f}} \mathbf{D}^{\mathrm{f}} (\mathbf{L}\mathbf{N}_e)\, \mathrm{d}A$$

$$\mathbf{C}^{\mathrm{f}}_{\mathrm{A2A2}} = \mathop{\mathrm{A}}_{e=1}^{\mathrm{EN}} \mathbf{C}^{\mathrm{f}}_{\mathrm{A2}e} = -\mathop{\mathrm{A}}_{e=1}^{\mathrm{EN}} \int\int_{\mathrm{A2}e} \mathbf{N}^{\mathrm{T}}_e \mathbf{n}^{\mathrm{f}} \mathbf{D}^{\mathrm{f}} (\mathbf{L}\mathbf{N}_e)\, \mathrm{d}A$$

$$\mathbf{C}^{\mathrm{c}} = \mathop{\mathrm{A}}_{e=1}^{\mathrm{EN}} \mathbf{C}^{m}_e = \mathop{\mathrm{A}}_{e=1}^{\mathrm{EN}} \int\int\int_{\Omega^{\mathrm{f}}_e} \hat{\mathbf{N}}^{\mathrm{T}}_e (\partial \mathbf{N}_e)\, \mathrm{d}\Omega$$

$$\mathbf{B}^{\mathrm{f}} = \mathop{\mathrm{A}}_{e=1}^{\mathrm{EN}} \mathbf{B}^{\mathrm{f}}_e = \mathop{\mathrm{A}}_{e=1}^{\mathrm{EN}} \int\int\int_{\Omega^{\mathrm{f}}_e} [(\mathbf{L}\mathbf{N}_e)^{\mathrm{T}} \mathbf{D}^{\mathrm{p}} \hat{\mathbf{N}}_e - \mathbf{N}^{\mathrm{T}}_e (\mathbf{L}^{\partial} \hat{\mathbf{N}}_e)]\, \mathrm{d}\Omega$$

$$\mathbf{B}^{\mathrm{f}}_{\Gamma^{\mathrm{fs}}\Gamma^{\mathrm{fs}}} = \mathop{\mathrm{A}}_{e=1}^{\mathrm{EN}} \mathbf{B}^{\mathrm{p}}_{\Gamma^{\mathrm{fs}}_e} = \mathop{\mathrm{A}}_{e=1}^{\mathrm{EN}} \int\int_{\Gamma^{\mathrm{fs}}_e} \mathbf{N}^{\mathrm{T}}_e \mathbf{n}^{\mathrm{f}} \mathbf{D}^{\mathrm{p}} \hat{\mathbf{N}}_e\, \mathrm{d}A$$

$$\mathbf{B}^{\mathrm{f}}_{\mathrm{A1A1}} = \mathop{\mathrm{A}}_{e=1}^{\mathrm{EN}} \mathbf{B}^{\mathrm{p}}_{\mathrm{A1}e} = -\mathop{\mathrm{A}}_{e=1}^{\mathrm{EN}} \int\int_{\mathrm{A1}e} \mathbf{N}^{\mathrm{T}}_e \mathbf{n}^{\mathrm{f}} \mathbf{D}^{\mathrm{p}} \hat{\mathbf{N}}_e\, \mathrm{d}A$$

$$\mathbf{B}^{\mathrm{f}}_{\mathrm{A2A2}} = \mathop{\mathrm{A}}_{e=1}^{\mathrm{EN}} \mathbf{B}^{\mathrm{p}}_{\mathrm{A2}e} = -\mathop{\mathrm{A}}_{e=1}^{\mathrm{EN}} \int\int_{\mathrm{A2}e} \mathbf{N}^{\mathrm{T}}_e \mathbf{n}^{\mathrm{f}} \mathbf{D}^{\mathrm{p}} \hat{\mathbf{N}}_e\, \mathrm{d}A$$

DOI: 10.1002/fld

$$\mathbf{M}^{\mathrm{s}} = \mathop{\mathrm{A}}_{e=1}^{\mathrm{EN}} \mathbf{M}_e^{\mathrm{s}} = \mathop{\mathrm{A}}_{e=1}^{\mathrm{EN}} \iiint_{\Omega_e^{\mathrm{s}}} \mathbf{N}_e^{\mathrm{T}} \mathbf{N}_e \, \mathrm{d}\Omega$$

$$\mathbf{C}^{\mathrm{s}} = \mathop{\mathrm{A}}_{e=1}^{\mathrm{EN}} \mathbf{C}_e^{\mathrm{s}} = \mathop{\mathrm{A}}_{e=1}^{\mathrm{EN}} \iiint_{\Omega_e^{\mathrm{s}}} \mathbf{N}_e^{\mathrm{T}} \mathbf{C}_d^{\mathrm{s}} \mathbf{N}_e \, \mathrm{d}\Omega$$

$$\mathbf{K}^{\mathrm{s}} = \mathop{\mathrm{A}}_{e=1}^{\mathrm{EN}} \mathbf{K}_e^{\mathrm{s}} = \mathop{\mathrm{A}}_{e=1}^{\mathrm{EN}} \iiint_{\Omega_e^{\mathrm{s}}} (\mathbf{L}\mathbf{N}_e)^{\mathrm{T}} \mathbf{D}^{\mathrm{s}} (\mathbf{L}\mathbf{N}_e) \, \mathrm{d}\Omega$$

$$\mathbf{K}^{\mathrm{s}}_{\Gamma^{\mathrm{fs}}\Gamma^{\mathrm{fs}}} = \mathop{\mathrm{A}}_{e=1}^{\mathrm{EN}} \mathbf{K}^{\mathrm{s}}_{\Gamma_e^{\mathrm{fs}}} = \mathop{\mathrm{A}}_{e=1}^{\mathrm{EN}} \iint_{\Gamma_e^{\mathrm{fs}}} \mathbf{N}_e^{\mathrm{T}} \mathbf{n}^{\mathrm{s}} \mathbf{D}^{\mathrm{s}} (\mathbf{L}\mathbf{N}_e) \, \mathrm{d}A$$

After introducing inflow and outflow conditions at both the inlet and outlet surfaces, we obtain the governing equations on the finite element formulations as below:

$$\mathbf{M}^{\mathrm{f}}_{11} \dot{\mathbf{V}}^{\mathrm{f}}_1 + \mathbf{C}^{\mathrm{f}}_{11}(\mathbf{V}^{\mathrm{f}}_1)\mathbf{V}^{\mathrm{f}}_1 + \mathbf{B}^{\mathrm{f}}_{11}\mathbf{P}^{\mathrm{f}}_1 + \mathbf{B}^{\mathrm{f}}_{12}\mathbf{P}^{\mathrm{f}}_2 + \mathbf{K}^{\mathrm{s}}_{\Gamma^{\mathrm{fs}}11}\mathbf{U}^{\mathrm{s}}_1 = \mathbf{R}^{\mathrm{f}}_1 \tag{51}$$

$$\mathbf{M}^{\mathrm{f}}_{21} \dot{\mathbf{V}}^{\mathrm{f}}_1 + \mathbf{C}^{\mathrm{f}}_{21}(\mathbf{V}^{\mathrm{f}}_1)\mathbf{V}^{\mathrm{f}}_1 + \mathbf{B}^{\mathrm{f}}_{12}\mathbf{P}^{\mathrm{f}}_1 + \mathbf{B}^{\mathrm{f}}_{22}\mathbf{P}^{\mathrm{f}}_2 = \mathbf{R}^{\mathrm{f}}_2 \tag{52}$$

$$\mathbf{C}^{\mathrm{c}}_{11}\mathbf{V}^{\mathrm{f}}_1 = \mathbf{R}^{\mathrm{c}}_1 \tag{53}$$

$$\mathbf{M}^{\mathrm{s}}_{11} \ddot{\mathbf{U}}^{\mathrm{s}}_1 + \mathbf{C}^{\mathrm{s}}_{11} \dot{\mathbf{U}}^{\mathrm{s}}_1 + \mathbf{K}^{\mathrm{s}}_{11}\mathbf{U}^{\mathrm{s}}_1 + \mathbf{B}^{\mathrm{f}}_{\Gamma^{\mathrm{fs}}11}\mathbf{P}^{\mathrm{f}}_1 + \mathbf{C}^{\mathrm{f}}_{\Gamma^{\mathrm{fs}}11}\mathbf{V}^{\mathrm{f}}_1 = \mathbf{R}^{\mathrm{s}}_1 \tag{54}$$

with

$$\mathbf{R}^{\mathrm{f}}_1 = \mathbf{M}^{\mathrm{f}}_{11} F^{\mathrm{f}}_1 + \mathbf{M}^{\mathrm{f}}_{12} F^{\mathrm{f}}_2 - \mathbf{M}^{\mathrm{f}}_{12} \dot{\mathbf{V}}^{\mathrm{f}}_2 - \mathbf{C}^{\mathrm{f}}_{12}\mathbf{V}^{\mathrm{f}}_2 \tag{55}$$

$$\mathbf{R}^{\mathrm{f}}_2 = \mathbf{M}^{\mathrm{f}}_{21} F^{\mathrm{f}}_1 + \mathbf{M}^{\mathrm{f}}_{22} F^{\mathrm{f}}_2 - \mathbf{M}^{\mathrm{f}}_{22} \dot{\mathbf{V}}^{\mathrm{f}}_2 - \mathbf{C}^{\mathrm{f}}_{22}\mathbf{V}^{\mathrm{f}}_2 \tag{56}$$

$$\mathbf{R}^{\mathrm{c}}_1 = -\mathbf{C}^{\mathrm{c}}_{12}\mathbf{V}^{\mathrm{f}}_2 \tag{57}$$

$$\mathbf{R}^{\mathrm{s}}_1 = \mathbf{M}^{\mathrm{s}}_{11} F^{\mathrm{s}}_1 \tag{58}$$

where $\mathbf{V}^{\mathrm{f}}_2$ is the known vector consisting of inflow condition $\mathbf{V}^{\mathrm{f}}_{\mathrm{A1}} = \mathbf{V}^{\mathrm{f}}_{\mathrm{inlet}}$ at the inlet and the convective outflow condition $\mathbf{V}^{\mathrm{f}}_{\mathrm{A2}} = \mathbf{V}^{\mathrm{f}}_{\mathrm{outlet}}$ at the outlet. We call the set of the governing equations as a monolithic coupling model (MCM) of the interaction between flow and the flow-induced vibration.

The incremental forms of MCM are used in order to have an effective solving action. Therefore, Equations (51)–(54) are stated as

$$\mathbf{M}^{\mathrm{f}}_{11} \Delta\dot{\mathbf{V}}^{\mathrm{f}}_1 + \mathbf{C}^{\mathrm{f}}_{11}(\Delta\mathbf{V}^{\mathrm{f}}_1)\Delta\mathbf{V}^{\mathrm{f}}_1 + \mathbf{B}^{\mathrm{f}}_{11}\Delta\mathbf{P}^{\mathrm{f}}_1 + \mathbf{B}^{\mathrm{f}}_{12}\Delta\mathbf{P}^{\mathrm{f}}_2 + \mathbf{K}^{\mathrm{s}}_{\Gamma^{\mathrm{fs}}11}\Delta\mathbf{U}^{\mathrm{s}}_1 = \Delta\mathbf{R}^{\mathrm{f}}_1 \tag{59}$$

$$\mathbf{M}^{\mathrm{f}}_{21} \Delta\dot{\mathbf{V}}^{\mathrm{f}}_1 + \Delta\mathbf{C}^{\mathrm{f}}_{21}(\Delta\mathbf{V}^{\mathrm{f}}_1)\Delta\mathbf{V}^{\mathrm{f}}_1 + \mathbf{B}^{\mathrm{f}}_{12}\Delta\mathbf{P}^{\mathrm{f}}_1 + \mathbf{B}^{\mathrm{f}}_{22}\Delta\mathbf{P}^{\mathrm{f}}_2 = \Delta\mathbf{R}^{\mathrm{f}}_2 \tag{60}$$

$$\mathbf{C}^{\mathrm{c}}_{11}\Delta\mathbf{V}^{\mathrm{f}}_1 = \Delta\mathbf{R}^{\mathrm{c}}_1 \tag{61}$$

$$\mathbf{M}^{\mathrm{s}}_{11} \Delta\ddot{\mathbf{U}}^{\mathrm{s}}_1 + \mathbf{C}^{\mathrm{s}}_{11} \Delta\dot{\mathbf{U}}^{\mathrm{s}}_1 + \mathbf{K}^{\mathrm{s}}_{11}\Delta\mathbf{U}^{\mathrm{s}}_1 + \mathbf{B}^{\mathrm{f}}_{\Gamma^{\mathrm{fs}}11}\Delta\mathbf{P}^{\mathrm{f}}_1 + \mathbf{C}^{\mathrm{f}}_{\Gamma^{\mathrm{fs}}11}\Delta\mathbf{V}^{\mathrm{f}}_1 = \Delta\mathbf{R}^{\mathrm{s}}_1 \tag{62}$$

DOI: 10.1002/fld

where the increments based on a generalized trapezoidal rule are defined as

$$\Delta\mathbf{V}_1^{\mathrm{f}} = \lambda\Delta t\Delta\dot{\mathbf{V}}_1^{\mathrm{f}} \tag{63}$$

$$\Delta\mathbf{U}_1^{\mathrm{s}} = \beta\Delta t\Delta\dot{\mathbf{U}}_1^{\mathrm{s}} = \beta\Delta t\Delta\mathbf{V}_1^{\mathrm{s}} \tag{64}$$

$$\Delta\mathbf{V}_1^{\mathrm{s}} = \Delta\dot{\mathbf{U}}_1^{\mathrm{s}} = \theta\Delta t\Delta\ddot{\mathbf{U}}_1^{\mathrm{s}} = \theta\Delta t\Delta\dot{\mathbf{V}}_1^{\mathrm{s}} \tag{65}$$

where λ, β and θ are referred to as the stability control parameters of the time integration for both the fluid and solid structures. Substituting Equations (63)–(65) into Equation (58)–(62) yields

$$\tilde{\mathbf{M}}_{11}^{\mathrm{f}}(\Delta\mathbf{V}_1^{\mathrm{f}})\Delta\mathbf{V}_1^{\mathrm{f}} + \mathbf{B}_{11}^{\mathrm{f}}\Delta\mathbf{P}_1^{\mathrm{f}} + \mathbf{B}_{12}^{\mathrm{f}}\Delta\mathbf{P}_2^{\mathrm{f}} + \hat{\mathbf{K}}_{\Gamma^{\mathrm{fs}}11}^{\mathrm{s}}\Delta\mathbf{V}_1^{\mathrm{s}} = \Delta\mathbf{R}_1^{\mathrm{f}} \tag{66}$$

$$\tilde{\mathbf{M}}_{21}^{\mathrm{f}}(\Delta\mathbf{V}_1^{\mathrm{f}})\Delta\mathbf{V}_1^{\mathrm{f}} + \mathbf{B}_{21}^{\mathrm{f}}\Delta\mathbf{P}_1^{\mathrm{f}} + \mathbf{B}_{22}^{\mathrm{f}}\Delta\mathbf{P}_2^{\mathrm{f}} = \Delta\mathbf{R}_2^{\mathrm{f}} \tag{67}$$

$$\mathbf{C}_{11}^{\mathrm{c}}\Delta\mathbf{V}_1^{\mathrm{f}} = \Delta\mathbf{R}_1^{\mathrm{c}} \tag{68}$$

$$\tilde{\mathbf{M}}_{11}^{\mathrm{s}}\Delta\mathbf{V}_1^{\mathrm{s}} + \mathbf{B}_{\Gamma^{\mathrm{fs}}11}^{\mathrm{f}}\Delta\mathbf{P}_1^{\mathrm{f}} + \mathbf{C}_{\Gamma^{\mathrm{fs}}11}^{\mathrm{f}}\Delta\mathbf{V}_1^{\mathrm{f}} = \Delta\mathbf{R}_1^{\mathrm{s}} \tag{69}$$

where the matrices with an over-caret are specified as

$$\tilde{\mathbf{M}}_{11}^{\mathrm{f}}(\Delta\mathbf{V}_1^{\mathrm{f}}) = \frac{\mathbf{M}_{11}^{\mathrm{f}}}{\lambda\Delta t} + \Delta\mathbf{C}_{11}^{\mathrm{f}}(\Delta\mathbf{V}_1^{\mathrm{f}}) \tag{70}$$

$$\tilde{\mathbf{M}}_{21}^{\mathrm{f}}(\Delta\mathbf{V}_1^{\mathrm{f}}) = \frac{\mathbf{M}_{21}^{\mathrm{f}}}{\lambda\Delta t} + \Delta\mathbf{C}_{21}^{\mathrm{f}}(\Delta\mathbf{V}_1^{\mathrm{f}}) \tag{71}$$

$$\tilde{\mathbf{M}}_{11}^{\mathrm{s}} = \frac{\mathbf{M}_{11}^{\mathrm{s}}}{\theta\Delta t} + \mathbf{C}_{11}^{\mathrm{s}} + \mathbf{K}_{11}^{\mathrm{s}}\beta\Delta t \tag{72}$$

$$\tilde{\mathbf{K}}_{\Gamma^{\mathrm{fs}}11}^{\mathrm{s}} = \mathbf{K}_{\Gamma^{\mathrm{fs}}11}^{\mathrm{s}}\beta\Delta t \tag{73}$$

4. SOLVING STRATEGY

To ensure the stabilization of the numerical procedure and to obtain the accurate solutions of flow in the dynamical FSI, we use the stabilized Newmark method [51] for the vibration of solid structure and the PMCA proposed by Hughes and Brooks [47] for fluid. A typical solution procedure of the time integration from τ to $\tau+\Delta t$ is shown as follows.

Step 1: *Predictors for fluid*. The Hughes' predictors for fluid are used as

$$\mathbf{V}_{1(\tau+\Delta t)}^{\mathrm{f}(m=0)} = \mathbf{V}_{1(\tau)}^{\mathrm{f}(m=0)} + (1-\lambda)\Delta t\dot{\mathbf{V}}_{1(\tau)}^{\mathrm{f}(m=0)} \tag{74}$$

$$\mathbf{P}_{1(\tau+\Delta t)}^{\mathrm{f}(m=0)} = \mathbf{P}_{1(\tau)}^{\mathrm{f}(m=0)} \tag{75}$$

$$\mathbf{P}_{2(\tau+\Delta t)}^{\mathrm{f}(m=0)} = \mathbf{P}_{2(\tau)}^{\mathrm{f}(m=0)} \tag{76}$$

where $\mathbf{V}_{1(\tau)}^{\mathrm{f}(m=0)}$, $\dot{\mathbf{V}}_{1(\tau)}^{\mathrm{f}(m=0)}$, $\mathbf{P}_{1(\tau)}^{\mathrm{f}(m=0)}$ and $\mathbf{P}_{2(\tau)}^{\mathrm{f}(m=0)}$ are the predicting setup values at iteration counter $m=0$. Bayoumi and Gadala [29], Dettmer and Perić [30] and Jansen *et al.* [52] suggested that the

DOI: 10.1002/fld

pressure should not be subjected to time integration because the continuity of flow was enforced in the variation formulation, instead it should be computed independently for each time increment.

Step 2: *Newmark's predictions for solid*. The Newmark's predictions of the time integration to solid are

$$\mathbf{U}^{\mathrm{s}(n+1)}_{1(\tau+\Delta t)} = \mathbf{U}^{\mathrm{s}(n)}_{1(\tau)} + \Delta t \mathbf{V}^{\mathrm{s}(n)}_{1(\tau)} + (\tfrac{1}{2}-\beta)\Delta t^2 \dot{\mathbf{V}}^{\mathrm{s}(n)}_{1(\tau)} + \beta \Delta t^2 \dot{\mathbf{V}}^{\mathrm{s}(n+1)}_{1(\tau+\Delta t)} \tag{77}$$

$$\mathbf{V}^{\mathrm{s}(n+1)}_{1(\tau+\Delta t)} = \mathbf{V}^{\mathrm{s}(n)}_{1(\tau)} + (1-\theta)\Delta t \dot{\mathbf{V}}^{\mathrm{s}(n)}_{1(\tau)} + \theta \Delta t \dot{\mathbf{V}}^{\mathrm{s}(n+1)}_{1(\tau+\Delta t)} \tag{78}$$

Step 3: *Structure solver*. It is easy to obtain the values of $\dot{\mathbf{V}}^{\mathrm{s}(n+1)}_{1(\tau+\Delta t)}$ and $\mathbf{V}^{\mathrm{s}(n+1)}_{1(\tau+\Delta t)}$ at time $\tau+\Delta t$ from Equations (77) and (78) as

$$\dot{\mathbf{V}}^{\mathrm{s}(n+1)}_{1(\tau+\Delta t)} = \frac{\mathbf{U}^{\mathrm{s}(n+1)}_{\tau+\Delta t} - (\mathbf{U}^{\mathrm{s}(n)}_{1(\tau)} + \Delta t \mathbf{V}^{\mathrm{s}(n)}_{1(\tau)} + (\frac{1}{2}-\beta)\Delta t^2 \dot{\mathbf{V}}^{\mathrm{s}(n)}_{1(\tau)})}{\beta \Delta t^2} \tag{79}$$

$$\mathbf{V}^{\mathrm{s}(n+1)}_{1(\tau+\Delta t)} = \mathbf{V}^{\mathrm{s}(n)}_{1(\tau)} + (1-\theta)\Delta t \dot{\mathbf{V}}^{\mathrm{s}(n)}_{1(\tau)} + \theta \Delta t \left[\frac{\mathbf{U}^{\mathrm{s}(n+1)}_{1(\tau+\Delta t)} - (\mathbf{U}^{\mathrm{s}(n)}_{1(\tau)} + \Delta t \mathbf{V}^{\mathrm{s}(n)}_{1(\tau)} + (\frac{1}{2}-\beta)\Delta t^2 \dot{\mathbf{V}}^{\mathrm{s}(n)}_{1(\tau)})}{\beta \Delta t^2} \right] \tag{80}$$

The restricted condition equation (50) on the interface is written as

$$\dot{\mathbf{U}}^{\mathrm{s}(n)}_{\Gamma^{\mathrm{fs}}(\tau)} = \mathbf{V}^{\mathrm{f}(m)}_{\Gamma^{\mathrm{fs}}(\tau)} \tag{81}$$

Substituting $\dot{\mathbf{V}}^{\mathrm{s}(n+1)}_{1(\tau+\Delta t)} = \ddot{\mathbf{U}}^{\mathrm{s}(n+1)}_{1(\tau+\Delta t)}$ and $\mathbf{V}^{\mathrm{s}(n+1)}_{1(\tau+\Delta t)} = \dot{\mathbf{U}}^{\mathrm{s}(n+1)}_{1(\tau+\Delta t)}$ into Equation (54) and replacing $\mathbf{V}^{\mathrm{f}(n)}_{\Gamma^{\mathrm{fs}}(\tau)}$ in $\mathbf{V}^{\mathrm{f}(n)}_{1(\tau)}$ of the fifth term of the left-hand side with $\dot{\mathbf{U}}^{\mathrm{s}(n)}_{\Gamma^{\mathrm{fs}}(\tau)} = \mathbf{V}^{\mathrm{f}(m)}_{\Gamma^{\mathrm{fs}}(\tau)}$, we can obtain the equation that is used to solve the displacement of solid $\mathbf{U}^{\mathrm{s}(n+1)}_{1(\tau+\Delta t)}$ at time $\tau+\Delta t$ as

$$\begin{aligned}
&\left[\frac{1}{\beta \Delta t^2}\mathbf{M}^{\mathrm{s}}_{11} + \frac{\theta}{\beta \Delta t}\mathbf{C}^{\mathrm{s}}_{11} + \frac{\theta}{\beta \Delta t}\mathbf{C}^{\mathrm{f}}_{\Gamma^{\mathrm{fs}}11} + \mathbf{K}^{\mathrm{s}}_{11} \right] \mathbf{U}^{\mathrm{s}(n+1)}_{1(\tau+\Delta t)} \\
&= \mathbf{R}^{\mathrm{s}(n+1)}_{1(\tau+\Delta t)} - \mathbf{B}^{\mathrm{f}}_{\Gamma^{\mathrm{fs}}11}\mathbf{P}^{\mathrm{f}(m)}_{1(\tau)} + \left[\frac{1}{\beta \Delta t^2}\mathbf{M}^{\mathrm{s}}_{11} + \frac{\theta}{\beta \Delta t}\mathbf{C}^{\mathrm{f}}_{\Gamma^{\mathrm{fs}}11} + \frac{\theta}{\beta \Delta t}\mathbf{C}^{\mathrm{s}}_{11} \right] \mathbf{U}^{\mathrm{s}(n)}_{1(\tau)} \\
&\quad + \left[\frac{1}{\beta \Delta t}\mathbf{M}^{\mathrm{s}}_{11} + \frac{\theta}{\beta}\mathbf{C}^{\mathrm{s}}_{11} + \frac{\theta}{\beta}\mathbf{C}^{\mathrm{f}}_{\Gamma^{\mathrm{fs}}11} - \mathbf{C}^{\mathrm{s}}_{11} - \mathbf{C}^{\mathrm{f}}_{\Gamma^{\mathrm{fs}}11} \right] \mathbf{V}^{\mathrm{s}(n)}_{1(\tau)} \\
&\quad + \left[\frac{(0.5-\beta)}{\beta}\mathbf{M}^{\mathrm{s}}_{11} + \frac{(0.5\theta-\beta)\Delta t}{\beta}\mathbf{C}^{\mathrm{s}}_{11} + \frac{(0.5\theta-\beta)\Delta t}{\beta}\mathbf{C}^{\mathrm{f}}_{\Gamma^{\mathrm{fs}}11} \right] \dot{\mathbf{V}}^{\mathrm{s}(n)}_{1(\tau)}
\end{aligned} \tag{82}$$

Rearranging above equation yields the solid displacements

$$\mathbf{U}^{\mathrm{s}(n+1)}_{1(\tau+\Delta t)} = (\mathbf{K}^{\mathrm{s}}_{11} + \hat{\mathbf{K}}^{\mathrm{s}}_{11})^{-1} \hat{\mathbf{R}}^{\mathrm{s}(n+1)}_{1(\tau+\Delta t)} \tag{83}$$

where

$$\hat{\mathbf{K}}_{11} = \frac{1}{\beta \Delta t^2}\mathbf{M}^{\mathrm{s}}_{11} + \frac{\theta}{\beta \Delta t}\mathbf{C}^{\mathrm{s}}_{11} + \frac{\theta}{\beta \Delta t}\mathbf{C}^{\mathrm{f}}_{\Gamma^{\mathrm{fs}}11}$$

DOI: 10.1002/fld

$$\hat{\mathbf{C}}^{\mathrm{s}}_{11}=\frac{1}{\beta\Delta t}\mathbf{M}^{\mathrm{s}}_{11}+\frac{\theta}{\beta}\mathbf{C}^{\mathrm{s}}_{11}+\frac{\theta}{\beta}\mathbf{C}^{\mathrm{f}}_{\Gamma^{\mathrm{fs}}11}-\mathbf{C}^{\mathrm{s}}_{11}-\mathbf{C}^{\mathrm{f}}_{\Gamma^{\mathrm{fs}}11}$$

$$\hat{\mathbf{M}}^{\mathrm{s}}_{11}=\frac{(0.5-\beta)}{\beta}\mathbf{M}^{\mathrm{s}}_{11}+\frac{(0.5\theta-\beta)\Delta t}{\beta}\mathbf{C}^{\mathrm{s}}_{11}+\frac{(0.5\theta-\beta)\Delta t}{\beta}\mathbf{C}^{\mathrm{f}}_{\Gamma^{\mathrm{fs}}11}$$

$$\hat{\mathbf{R}}^{\mathrm{s}(n+1)}_{1(\tau+\Delta t)}=\mathbf{R}^{\mathrm{s}(n+1)}_{1(\tau+\Delta t)}-\mathbf{B}^{\mathrm{f}}_{\Gamma^{\mathrm{fs}}11}\mathbf{P}^{\mathrm{f}(m)}_{1(\tau)}+\hat{\mathbf{K}}^{\mathrm{s}}_{11}\mathbf{U}^{\mathrm{s}(n)}_{1(\tau)}+\hat{\mathbf{C}}^{\mathrm{s}}_{11}\mathbf{V}^{\mathrm{s}(n)}_{1(\tau)}+\hat{\mathbf{M}}^{\mathrm{s}}_{11}\dot{\mathbf{V}}^{\mathrm{s}(n)}_{1(\tau)}$$

Substituting Equation (83) into Equations (79) and (80) yields the solutions of the vibration velocity and acceleration of solid structure at time $\tau+\Delta t$.

Step 4: *Solutions for fluid*. From Equation (68), we directly obtain the increments of flow velocity as

$$\Delta\mathbf{V}^{\mathrm{f}(m)}_{1(\tau+\Delta t)}=(\mathbf{C}^{\mathrm{c}}_{11})^{-1}\Delta\mathbf{R}^{\mathrm{c}(m)}_{1(\tau+\Delta t)} \tag{84}$$

Substituting Equation (84) into Equations (66) and (67) yields two equations for solving $\mathbf{P}^{\mathrm{f}(n+1)}_{1(\tau+\Delta t)}$ and $\mathbf{P}^{\mathrm{f}(n+1)}_{2(\tau+\Delta t)}$

$$\mathbf{B}^{\mathrm{f}}_{11}\Delta\mathbf{P}^{\mathrm{f}(m)}_{1(\tau+\Delta t)}+\mathbf{B}^{\mathrm{f}}_{12}\Delta\mathbf{P}^{\mathrm{f}(m)}_{2(\tau+\Delta t)}=\Delta\hat{\mathbf{R}}^{\mathrm{f}(m)}_{1(\tau+\Delta t)} \tag{85}$$

$$\mathbf{B}^{\mathrm{f}}_{21}\Delta\mathbf{P}^{\mathrm{f}(m)}_{1(\tau+\Delta t)}+\mathbf{B}^{\mathrm{f}}_{22}\Delta\mathbf{P}^{\mathrm{f}(m)}_{2(\tau+\Delta t)}=\Delta\mathbf{R}^{\mathrm{f}(m)}_{2(\tau+\Delta t)} \tag{86}$$

where

$$\Delta\hat{\mathbf{R}}^{\mathrm{f}(m)}_{1(\tau+\Delta t)}=\Delta\mathbf{R}^{\mathrm{f}(m)}_{1(\tau+\Delta t)}-\hat{\mathbf{K}}^{\mathrm{s}}_{\Gamma^{\mathrm{fs}}11}\Delta\mathbf{V}^{\mathrm{s}(n+1)}_{1(\tau+\Delta t)}-\tilde{\mathbf{M}}^{\mathrm{f}}_{11}[(\mathbf{C}^{\mathrm{c}}_{11})^{-1}\Delta\mathbf{R}^{\mathrm{c}(m)}_{1(\tau+\Delta t)}](\mathbf{C}^{\mathrm{c}}_{11})^{-1}\Delta\mathbf{R}^{\mathrm{c}(m)}_{1(\tau+\Delta t)}$$

$$\Delta\hat{\mathbf{R}}^{\mathrm{f}(m)}_{2(\tau+\Delta t)}=\Delta\mathbf{R}^{\mathrm{f}(m)}_{2(\tau+\Delta t)}-\tilde{\mathbf{M}}^{\mathrm{f}}_{21}[(\mathbf{C}^{\mathrm{c}}_{11})^{-1}\Delta\mathbf{R}^{\mathrm{c}(m)}_{1(\tau+\Delta t)}](\mathbf{C}^{\mathrm{c}}_{11})^{-1}\Delta\mathbf{R}^{\mathrm{c}(m)}_{1(\tau+\Delta t)}$$

Step 5: *Correction for fluid*. Flow velocity and pressure at time $\tau+\Delta t$ are finally corrected as

$$\mathbf{V}^{\mathrm{f}(m+1)}_{1(\tau+\Delta t)}=\mathbf{V}^{\mathrm{f}(m)}_{1(\tau+\Delta t)}+\lambda\Delta t\Delta\dot{\mathbf{V}}^{\mathrm{f}(m)}_{1(\tau+\Delta t)} \tag{87}$$

$$\mathbf{P}^{\mathrm{f}(m+1)}_{1(\tau+\Delta t)}=\mathbf{P}^{\mathrm{f}(m)}_{1(\tau+\Delta t)}+\Delta\mathbf{P}^{\mathrm{f}(m)}_{1(\tau+\Delta t)} \tag{88}$$

$$\mathbf{P}^{\mathrm{f}(m+1)}_{2(\tau+\Delta t)}=\mathbf{P}^{\mathrm{f}(m)}_{2(\tau+\Delta t)}+\Delta\mathbf{P}^{\mathrm{f}(m)}_{2(\tau+\Delta t)} \tag{89}$$

Step 6: *Convective outflow condition at the outlet*. The boundary condition of $\mathbf{V}^{\mathrm{f}(m+1)}_{\mathrm{outlet}(\tau+\Delta t)}$ at the outlet surface A2 is treated as a convective outflow condition. Following the Reference [4], this can be written as

$$\mathbf{V}^{\mathrm{f}(m+1)}_{\mathrm{outlet}(\tau+\Delta t)}(N_x)=-\frac{\bar{\mathbf{V}}^{\mathrm{f}(m)}_{\mathrm{inlet}(\tau+\Delta t)}\Delta t}{\Delta x}[\mathbf{V}^{\mathrm{f}(m)}_{\mathrm{outlet}(\tau+\Delta t)}(N_x)-\mathbf{V}^{\mathrm{f}(m)}_{\mathrm{outlet}(\tau+\Delta t)}(N_x-1)]$$
$$+\mathbf{V}^{\mathrm{f}(m)}_{\mathrm{outlet}(\tau+\Delta t)}(N_x) \tag{90}$$

where N_x is the number of the grid lines in the streamline direction and $\bar{\mathbf{V}}^{\mathrm{f}(m)}_{\mathrm{inlet}(\tau+\Delta t)}$ is the mean flow velocity at the inlet surface.

DOI: 10.1002/fld

5. NUMERICAL EXAMPLES

5.1. Example 1: 3-D lid-driven square cavity flow

The lid-driven square cavity flow is a typical benchmark problem to validate new numerical techniques (see, for example, References [25, 27, 53]). This example is also chosen to verify the model and numerical methodology developed here. A uniform mesh of $51 \times 51 \times 51$ is used in present study. The stiffness of the solid walls is sufficiently large in order to invalidate the interaction between fluid and solid structure. The computed velocity fields and the pressure contours for flow of the Reynolds numbers of 1000, 400 and 100, respectively, are shown in Figures 3 and 4. The numerical results from Reference [53] based on the DQ method and Reference [27] based on the least-square FEM are also exhibited in Figures 3 and 4 for purpose of comparison. It is seen that

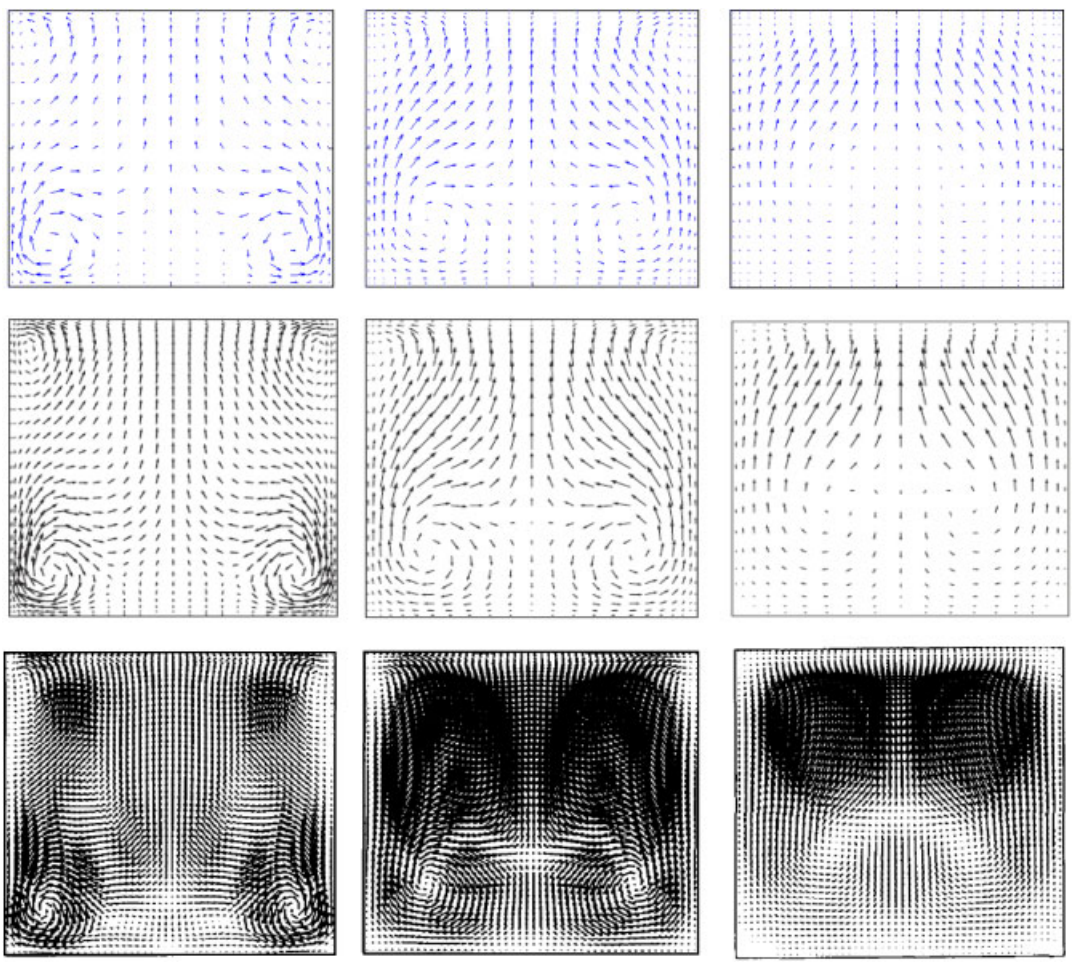

Figure 3. Comparisons of velocity fields at $x = 0.5$ for Reynolds numbers of 1000(left), 400(middle) and 100(right). Top: present paper, middle: Reference [53] and bottom: Reference [27].

DOI: 10.1002/fld

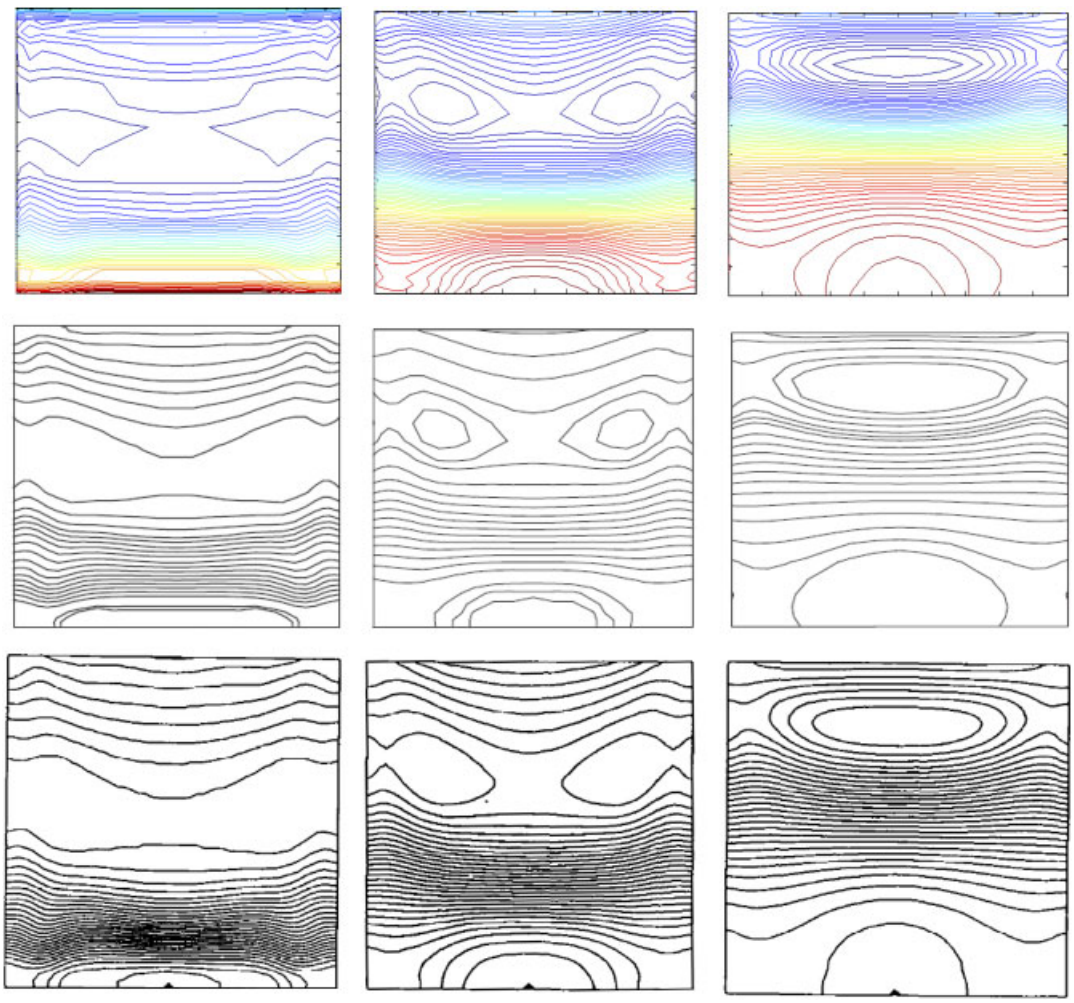

Figure 4. Comparisons of pressure fields at $x=0.5$ for Reynolds numbers of 1000(left), 400(mid) and 100(right). Top: present paper, middle: Reference [53] and bottom: Reference [27].

our numerical results agree well with those of References [27, 53], and a significant advantage of our method is monolithically extending solid dynamics into flow.

5.2. *Example 2: Flow in a hydro-turbine with dynamical FSI*

5.2.1. Geometry of flow passage. The flow geometry in this example is a blade passage of a model unit of a real hydro-turbine, which was used in Reference [43] by the same authors. For the sake of convenience and completeness, we give a brief description of the main specifications of this hydro-turbine rig. The machine has a 450 mm diameter turbine runner and 10 blades, 23 moving and stay vanes. The lengths of the curved edges of the blade are $L_1=166$ mm at the inlet and $L_2=281$ mm at the outlet. The lengths of the crossing lines of the blade with the crown and the

DOI: 10.1002/fld

band are $L_3 = 130\,\text{mm}$ and $L_4 = 197\,\text{mm}$, respectively. The pitches of the blades are $S_1 = 69\,\text{mm}$ at the crown and $S_2 = 102\,\text{mm}$ at the band. The mean chord length of the blade is $L = 157.3\,\text{mm}$. The fluid domain in the present study is surrounded by the surfaces of A1–A6, in which the surfaces of A1 and A2 are the inlet and outlet of the passage, and the surfaces of A3–A6 are the interfaces between fluid and solid. The main components of the turbine blade passage and their geometrical configurations are shown in Figure 1, while the details of the test rig and test implementation on the turbine unit can be found in Reference [43].

Two blades are only considered as deformable structure, whose Young's modulus is 2500 MPa, Poisson's ratio 0.384 and the mass density $1280\,\text{kg/m}^3$. Other solid components except these two blades are treated as rigid body. So, the elastic blades are rigidly attached to the crow and the band at the two ends of the blade.

5.2.2. Meshes. The fluid domain is discretized by using a multilinear velocity/constant pressure element used in References [25, 47]. The elements are of eight-noded hexahedron form and the structured mesh is used for fluid and solid domains. The size of the fluid element is generally controlled with the grid intensity of $L_2 \times L_4 \times S_2 = 200 \times 140 \times 52$, while the meshes near the solid walls are locally densified. The total number of the fluid elements is approximately 1.8 millions. The elements for each blade are 84 000. The nodal number on the two sides of the deformable interfaces between fluid and solid is the same. The elements for the domains are shown in Figure 5 (red presents elements attached to the solid walls).

5.2.3. Boundary conditions and control parameters. The known inflow velocity distributions on the inlet surface of A1 at each time step Δt are taken from Reference [43]. The convective outflow conditions at the outlet surface of A2 are correspondingly computed in time using Equation (90). No-slip rigid wall conditions are applied on the surfaces of A5 and A6. The deformable interfaces of A3 and A4 are used as the periodical boundaries in the pitchwise direction of the blade cascades.

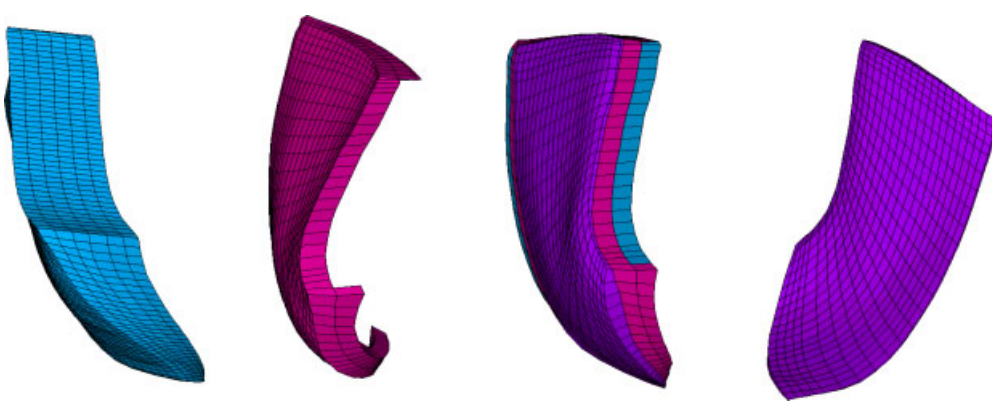

Figure 5. Rarefied elements attached to the domains.

DOI: 10.1002/fld

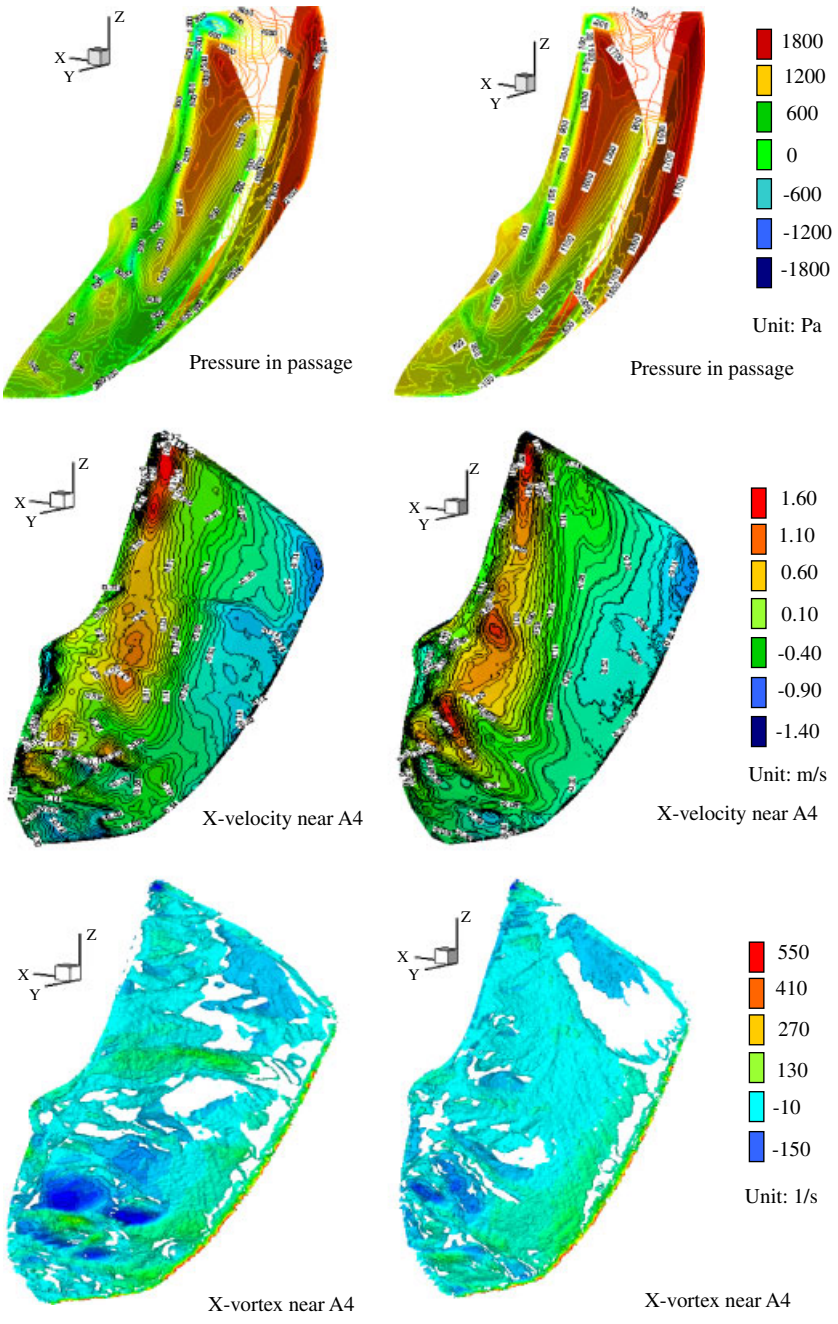

Figure 6. Comparisons of pressure, velocity and X-vortex iso-surface at time of $t/T = 7.00$.

DOI: 10.1002/fld

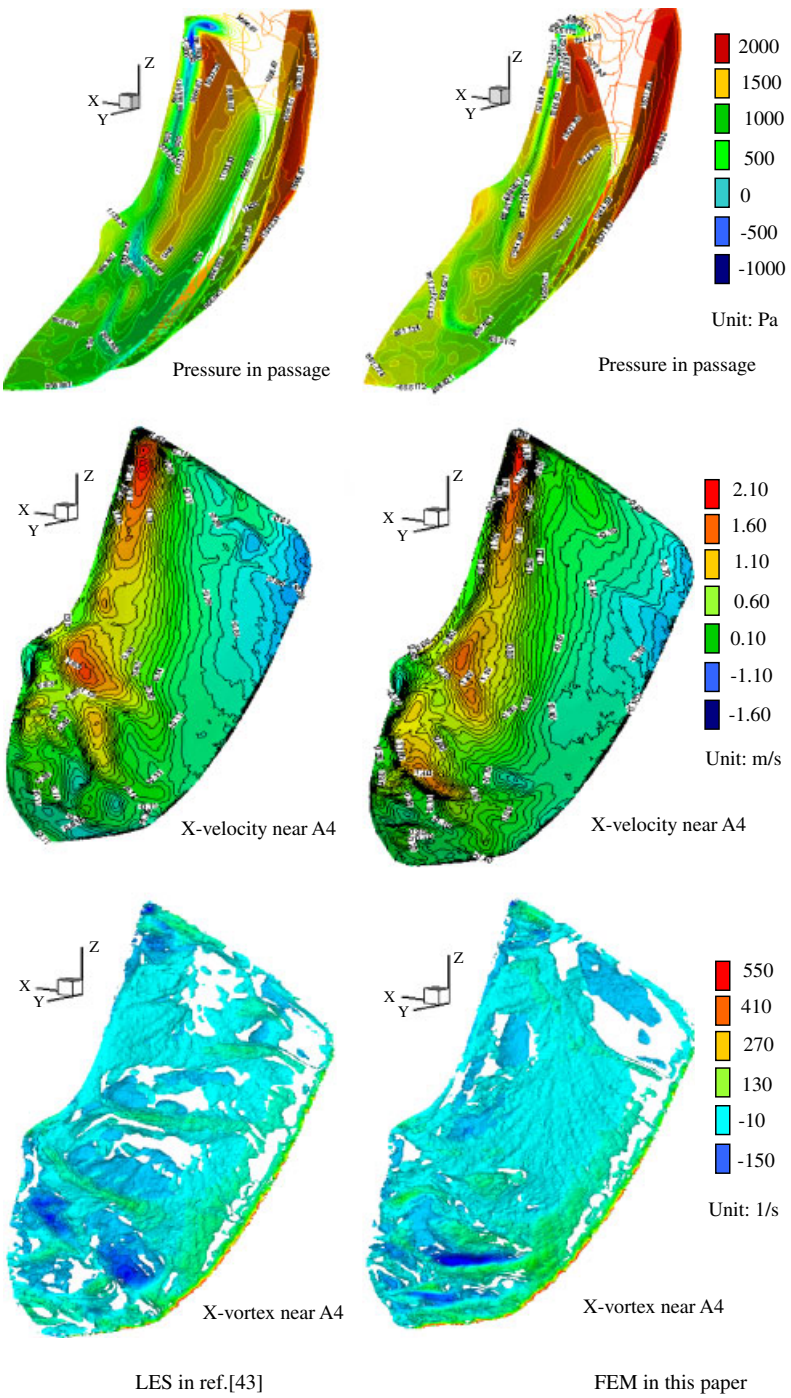

Figure 7. Comparisons of pressure, velocity and X-vortex iso-surface at time of $t/T = 8.35$.

DOI: 10.1002/fld

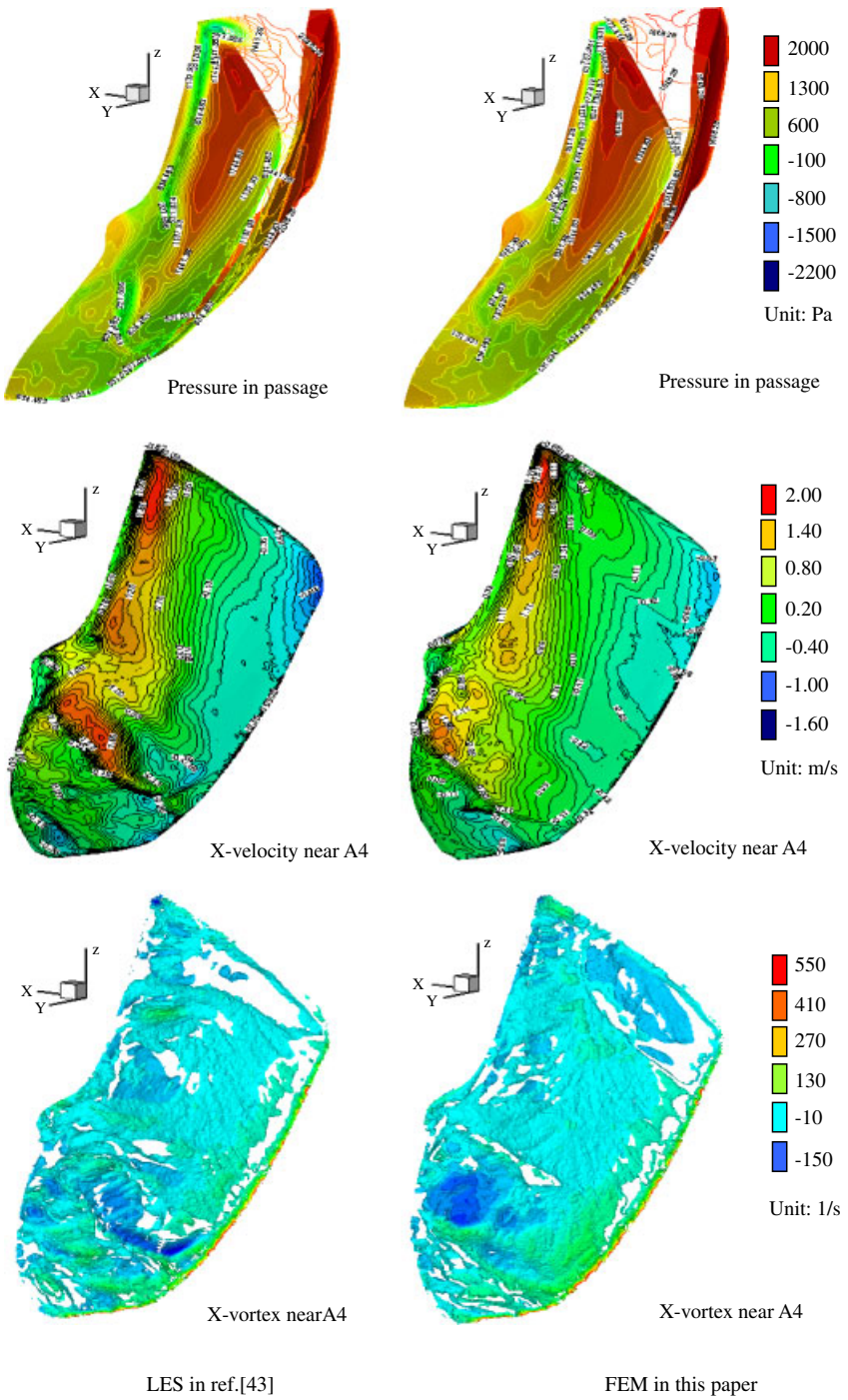

Figure 8. Comparisons of pressure, velocity and X-vortex iso-surface at time of $t/T = 9.10$.

DOI: 10.1002/fld

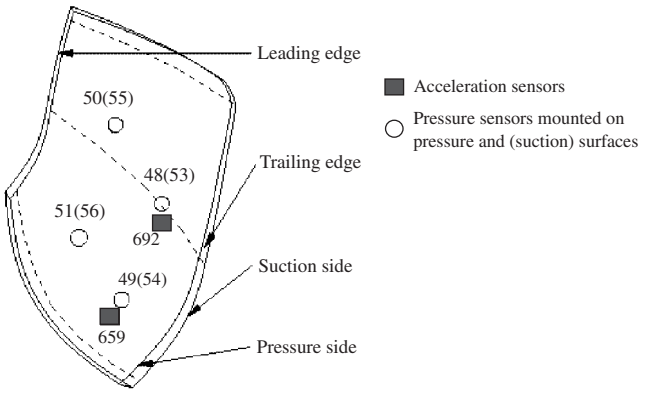

Figure 9. Pressure and acceleration sensors mounted at the blade.

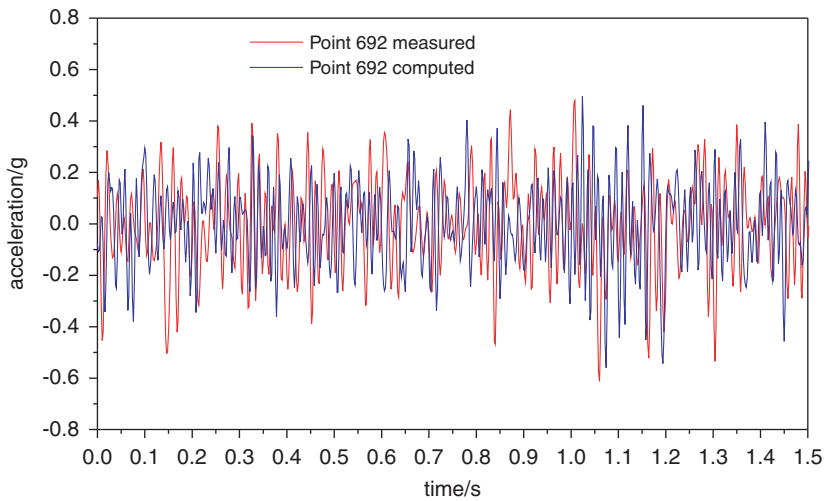

Figure 10. Comparisons of measured and computed acceleration histories at point 692 (history is filtered from frequency range of 0.1 Hz–80 Hz).

The opening of the guide vanes is taken as 22 mm. The incident angle of the inflow is about 39° and the mean velocity of the inflow based on the inlet surface of A1 is $\bar{V}_{\infty}^{\mathrm{f}} = 1\,\mathrm{m/s}$. The sweeping period of flow from the inlet to the outlet is $T = L/\bar{V}_{\infty}^{\mathrm{f}} = 0.1573\,\mathrm{s}$. The flow Reynolds number is $Re = \bar{V}_{\infty}^{\mathrm{f}} L/v = 148\,400$ (v is kinetic viscosity). The stabilized control parameters for fluid and solid structure are equally taken as $\lambda = \theta = 0.5$ and $\beta = \frac{1}{6}$.

The size of the time step for flow is taken as $\Delta t^{\mathrm{f}} = 0.0004\,\mathrm{s}$ in simulation and time duration is 1.573 s, which is 10 times of the sweeping period; while the size of the time step for the structure vibration is taken as $\Delta t^{\mathrm{s}} = 0.004\,\mathrm{s}$, being 10 times of the flow step. This staggered solving strategy in time is to ensure numerical stabilization without losing accuracy of the vibration solution.

DOI: 10.1002/fld

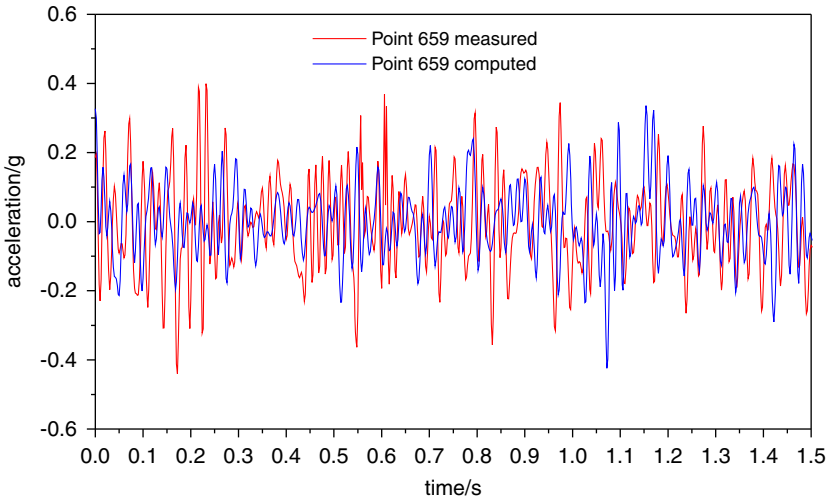

Figure 11. Comparisons of measured and computed acceleration histories at point 659 (history is filtered from frequency range of 0.1 Hz–80 Hz).

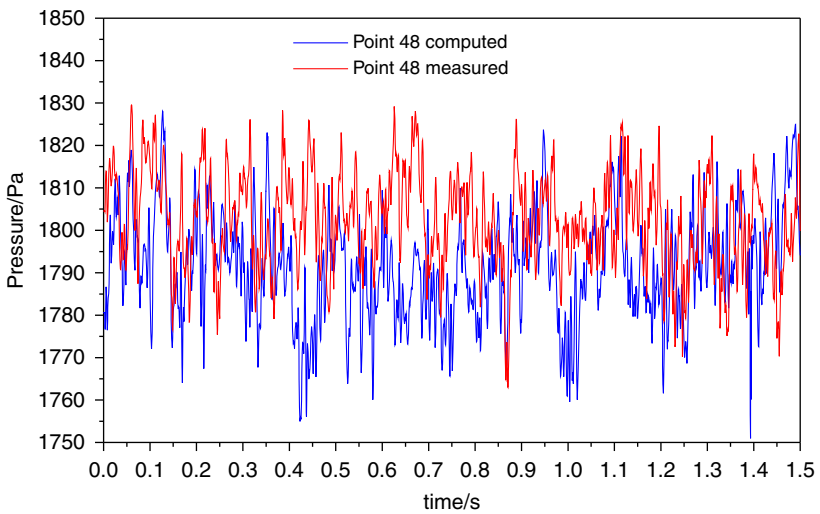

Figure 12. Comparisons of measured and computed pressure histories at point 48 on pressure side.

5.2.4. Correction of meshes near vibrating walls. The peak displacement of the flow-induced blade vibration in this example is about 0.01 mm, while the minimum size of the elements near the vibrating walls is about 0.5 mm, which is 50 times of the peak displacement. It implies that the fluid mesh distortion caused by the wall vibration is small against the element scale. Therefore, the correction of the meshes in time is not required in the computation.

DOI: 10.1002/fld

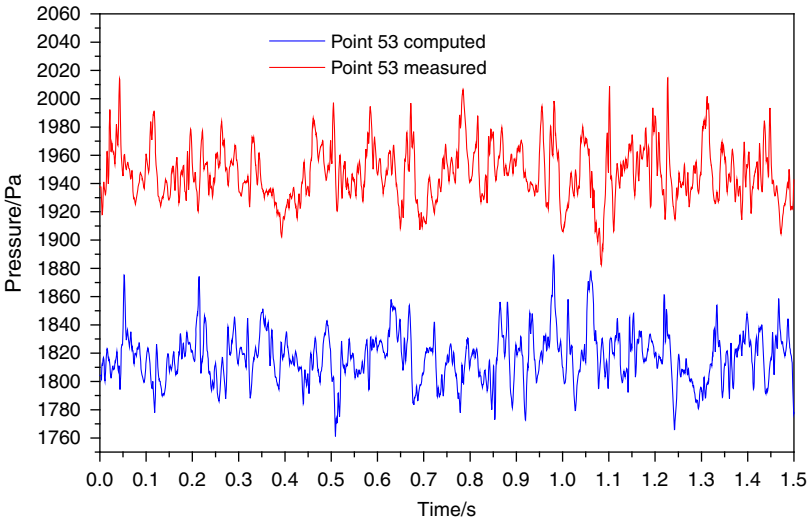

Figure 13. Comparisons of measured and computed pressure histories at point 53 on suction side.

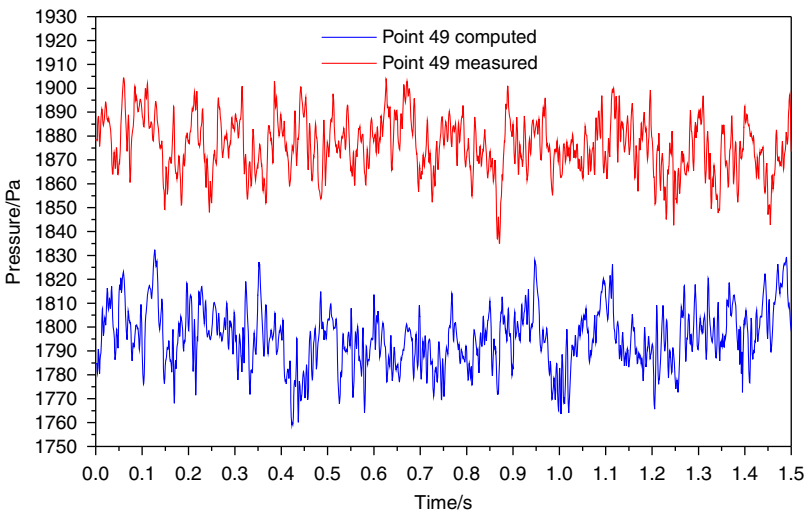

Figure 14. Comparisons of measured and computed pressure histories at point 49 on pressure side.

5.2.5. Flow fields in the blade passage. The numerical computations have been performed using the authors' own code as a solver. The software of TECPLOT® is used as a post-processor for analyzing the computing data and ANSYS® as a pre-processor for obtaining the nodal coordinate information of the elements. The rotation of the runner is not considered in this example in order to better investigate intrinsic features of turbulences in the strongly distorted passage with the vibrations of the blades.

DOI: 10.1002/fld

The snapshot comparisons of the pressure distributions, the flow velocity and vortex in x-direction (in Cartesian reference) at the regions near the vibrating walls are shown in Figures 6–8, at three dimensionless times of $t/T = 7.00$, 8.35 and 9.10, respectively. It is seen that the general tendencies of pressure and velocity distribution are in good agreement with those by LES in Reference [43]. A strong vortex at the leading zone of the passage is clearly demonstrated and the features of the flow field in this zone are roughly the same except in the lower and the right upper zones of the passage. As flow enters into the lower part zone of the passage, the flow structures become more complicated due to strongly curved geometry of the passage, and the evolution of the vortex is fully developed. The variations of the distribution of the flow patterns between LES in Reference [43] and FEM in this paper gradually become clear because the flow turbulence in this zone is significantly strengthened.

5.2.6. Pressure and vibrating acceleration at specified points of blade. Laboratory experiment for the corresponding case was carried out to measure the pressure at the blade and the acceleration of the blade vibration at the specified locations. The test rig used is a turbine model unit (see Reference [43]). Figure 9 shows that eight pressure transducers of the type LL-072-25A manufactured by Kulite Company and two acceleration transducers were mounted at the specified locations of the blade. The computed and measured accelerations and pressure at the specified locations are shown in Figures 10–15. It is seen that the computed acceleration agrees well with the measurements. A good agreement between the computed and measured tendencies of the pressure variation with time was also obtained, though the numerical model systemically underestimates the pressure. The maximum relative error between the computed and measured pressure is about 8%. Figure 16 is a quantitative comparison of the time-averaged pressures at the specified locations. It is seen that the numerical results obtained using the methodology proposed in the present study have a reasonable tendency compared with measured results, although the time-averaged computed pressures are systemically less than the measured with the maximum variation being less than about 100 Pa,

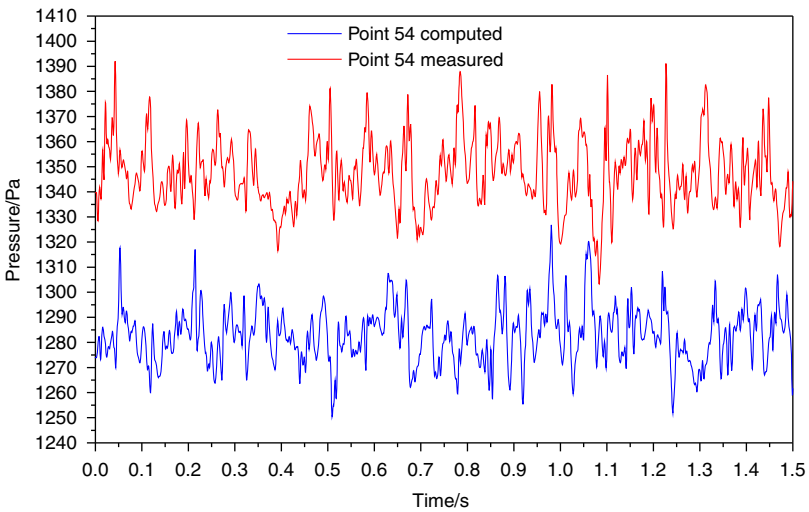

Figure 15. Comparisons of measured and computed pressure histories at point 54 on suction side.

DOI: 10.1002/fld

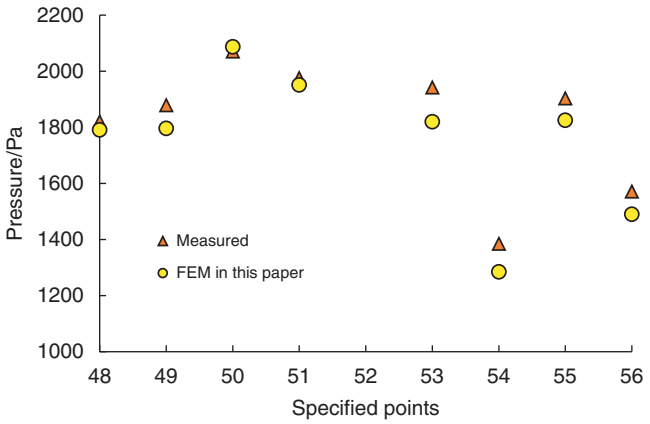

Figure 16. Comparisons of time-averaged pressures at specified points on two sides of blade.

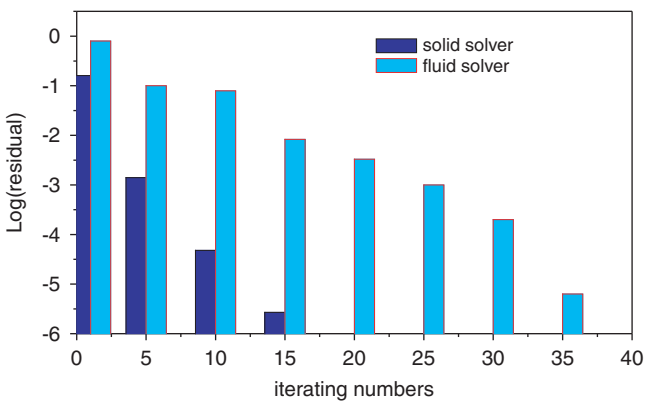

Figure 17. Iterating convergence behaviors within a typical time step.

or, nearly 1 cm head. The reason is that the test water head supplied is slightly bigger. Figure 17 exhibits convergence behaviors of both flow and solid structures in simulation.

6. CONCLUSIONS

A fully coupled mathematical model is established to describe turbulent flow in strongly curved turbine blade passage with the dynamical FSI due to the flow-induced blade vibrations. The model is created by combining the incompressible viscous Navier–Stokes equations with the elastically small deformation vibration equations by using hybrid generalized variational principle of fluid and solid mechanics. The solving strategy is based on the stabilized finite element formulations. The Newmark method and the PMCA proposed by Hughes are employed in the time integration for solid and fluid, respectively. The time-staggered iteration scheme used in the paper can effectively

DOI: 10.1002/fld

suppress numerical dissipation in simulation for the dynamical FSI in small deforming structure vibrating problems and ensure numerical iteration convergence. Good agreement between the computation and measurements indicates that the model and methodology developed in this study can be applied to simulate the turbulent flow involving a complex geometry and the flow-induced structure vibration with the dynamical FSI.

ACKNOWLEDGEMENTS

The authors thank the National Natural Science Foundation of China (NSFC) [Grant no. 50839003 and 50579025] for financial supports of this research. The comments made by the anonymous reviewers greatly improved the quality of the paper.

REFERENCES

1. Weaver DS, Ziada S, Au-Yang MK, Chen SS, Paidoussis MP, Pettigrew MJ. Flow-induced vibration in power and process plants components—progress and prospects. *ASME Journal of Pressure Vessel Technology* 2000; **122**:339–348.
2. Blevins RD. *Flow Induced Vibrations* (2nd edn). van Nostrand Reinhold: New York, NY, 1990.
3. Wu XH, Durbin PA. Evidence of longitudinal vortices evolved from distorted wakes in a turbine passage. *Journal of Fluid Mechanics* 2001; **446**:199–228.
4. Kalitzin G, Wu XH, Durbin PA. DNS of fully turbulent flow in a LPT passage. *International Journal of Heat and Fluid Flow* 2003; **24**:636–644.
5. Wissink JG. DNS of separating, low Reynolds number flow in a turbine cascade with incoming wakes. *International Journal of Heat and Fluid Flow* 2003; **24**:626–635.
6. Rodi W. DNS and LES of some engineering flows. *Fluid Dynamics Research* 2006; **38**:145–173.
7. Moin P, Mahesh K. Direct numerical simulation: a tool in turbulence research. *Annual Review of Fluid Mechanics* 1998; **30**:539–578.
8. Wissink JG, Rodi W. Direct numerical simulation of flow and heat transfer in a turbine cascade with incoming wakes. *Journal of Fluid Mechanics* 2006; **569**:209–247.
9. Jordan SA. A large-eddy simulation methodology in generalized curvilinear coordinates. *Journal of Computational Physics* 1999; **148**:322–340.
10. Morinishi Y, Lund TS, Vasilyev OV, Moin P. Fully conservative higher order finite difference schemes for incompressible flow. *Journal of Computational Physics* 1998; **143**:90–124.
11. Moin P. Advances in large eddy simulation methodology for complex flows. *International Journal of Heat and Fluid Flow* 2002; **24**:710–720.
12. Conway S, Caraeni D, Fuchs L. Large eddy simulation of the flow through the blades of a swirl generator. *International Journal of Heat and Fluid Flow* 2002; **21**:664–673.
13. Manna M, Benocci C, Simons E. Large eddy simulation of turbulent flows via domain decomposition techniques. Part 1: theory. *International Journal for Numerical Methods in Fluids* 2005; **48**:367–395.
14. Benocci C, Giammanco R, Manna M, Simons E. Large eddy simulation of turbulent flows via domain decomposition techniques. Part II: applications. *International Journal for Numerical Methods in Fluids* 2005; **48**:397–422.
15. Tyagi M, Acharya S. Large eddy simulation of turbulent flows in complex and moving rigid geometries using the immersed boundary method. *International Journal for Numerical Methods in Fluids* 2005; **48**:691–722.
16. Kravchenko AG, Moin P, Moser R. Zonal embedded grids for numerical simulations of wall-bounded turbulent flows. *Journal of Computational Physics* 1996; **127**:412–423.
17. Namkoong K, Choi HG, Yoo JY. Computation of dynamic fluid–structure interaction in two dimensional laminar flows using combined formulation. *Journal of Fluids and Structures* 2005; **20**:51–69.
18. Sarrate J, Huerta A, Donea J. Arbitrary Lagrangian Eulerian formulation for fluid–rigid body interaction. *Computer Methods in Applied Mechanics and Engineering* 2001; **190**:3171–3188.
19. Souli M, Ouahsine A, Lewin L. ALE formulation for fluid structure interaction problems. *Computer Methods in Applied Mechanics and Engineering* 2000; **190**:659–675.

DOI: 10.1002/fld

20. Peskin CS. Numerical analysis of blood flow in the heart. *Journal of Computational Physics* 1977; **25**:220–252.
21. Kim J, Kim D, Choi H. An immersed-boundary finite-volume method for simulations of flow in complex geometries. *Journal of Computational Physics* 2001; **171**:132–150.
22. Iaccarino G, Verzicco R. Immersed boundary technique for turbulent flow simulations. *Applied Mechanics Reviews* 2003; **56**:331–347.
23. Tseng Y-H, Ferziger JH. A ghost-cell immersed boundary method for flow in complex geometry. *Journal of Computational Physics* 2003; **192**:593–623.
24. Shin S, Bae SY, Kim IC, Kim YJ, Goo JS. Computation of flow over a flexible plate using the hybrid Cartesian/immersed boundary method. *International Journal for Numerical Methods in Fluids* 2007; **55**:263–282.
25. Tezduyar TE. Stabilized finite element formulations for incompressible flow computation. *Advances in Applied Mechanics* 1991; **28**:1–44.
26. Reddy JN. *An Introduction to the Finite Element Method* (2nd edn). McGraw-Hill: New York, 1993; 488–492.
27. Jiang BN, Lin TL, Povinelli LA. Large-scale computation of incompressible viscous flow by least-squares finite element method. *Computer Methods in Applied Mechanics and Engineering* 1994; **114**:213–321.
28. Tezduyar TE. Computation of moving boundaries and interfaces and stabilization parameters. *International Journal for Numerical Methods in Fluids* 2003; **43**:555–575.
29. Bayoumi HN, Gadala MS. A complete finite element treatment for the fully coupled implicit ALE formulation, *Computational Mechanics* 2004; **33**(6):435–452.
30. Dettmer W, Perić D. A computational framework for fluid–structure interaction: finite element formulation and applications. *Computer Methods in Applied Mechanics and Engineering* 2006; **195**:5757–5779.
31. Tezduyar TE. Finite elements in fluids: stabilized formulations and moving boundaries and interfaces. *Computers and Fluids* 2007; **36**:191–206.
32. Tezduyar TE. Finite elements in fluids: special methods and enhanced solution techniques. *Computers and Fluids* 2007; **36**:207–223.
33. Tezduyar TE, Sathe S. Modelling of fluid–structure interaction with the space–time finite element: solution techniques. *International Journal for Numerical Methods in Fluids* 2007; **54**:855–900.
34. Teixeira PRF, Awruch AM. Numerical simulation of fluid–structure interaction using the finite element method. *Computers and Fluids* 2005; **34**:249–273.
35. Guruswamy GP, Byun C. Fluid–structure interaction using Navier–Stokes flow equations coupled with shell finite element structure. *AIAA-93-3087*, 1993.
36. Guruswamy GP, Byun C. Direct coupling of Euler flow equations with plate finite element structures. *AIAA Journal* 1994; **33**(2):375–377.
37. Garica JA, Guruswamy GP. Aeroelastic analysis of transonic wings using Navier–Stokes equations and a nonlinear beam finite element model. *AIAA-1999-1215*, 1999.
38. Ishiharal D, Yoshimura S. A monolithic approach for interaction of incompressible viscous fluid and an elastic body based on fluid pressure Poisson equation. *International Journal for Numerical Methods in Engineering* 2005; **64**:167–203.
39. Chen XJ, Wu YSH. Review of hydroelasticity theories for global response of marine structures. *Ocean Engineering* 2006; **33**:439–457.
40. Tai CH, Bals B, Zhao Y, Liew KM. An efficient parallel computation of unsteady incompressible viscous flow with elastic moving and compliant boundaries on unstructured grids. *International Journal for Numerical Methods in Engineering* 2005; **64**:2072–2104.
41. Tai CH, Zhao Y, Liew KM. Parallel-multigrid computation of unsteady incompressible viscous flows using a matrix-free implicit method and high-resolution characteristics-based scheme. *Computer Methods in Applied Mechanics and Engineering* 2005; **194**:3949–3983.
42. Liew KM, Wang WQ, Zhang LX, He XQ. A computational approach for predicting the hydroelasticity of flexible structures based on the pressure Poisson equation. *International Journal for Numerical Methods in Engineering* 2007; **72**(13):1560–1583.
43. Zhang LX, Guo Y, Wang WQ. Large eddy simulation of turbulent flow in a true 3D Francis hydro turbine passage with dynamical fluid–structure interaction. *International Journal for Numerical Methods in Fluids* 2007; **54**:517–541.
44. Zhang LX, Wang WQ, Guo Y. Numerical simulation of flow features and energy exchanging physics in near-wall region with fluid–structure interaction. *International Journal of Modern Physics B* 2008; **22**(6):651–669.
45. Matthies HG. Partitioned analysis of coupled systems. *Fifth International Conference on Computation of Shell and Spatial Structure*, Salzburg, Austria, 2005.

DOI: 10.1002/fld

46. Bathe KJ, Zhang H, Wang WH. Finite element analysis of incompressible and compressible fluid flows with free surfaces and structural interactions. *Computers and Structures* 1995; **56**:193–213.
47. Brooks AN, Hughes TJR. Streamline upwind/Petrov–Galerkin formulations for convection-dominated flows with particular emphasis on the incompressible Naiver–Stokes equations. *Computer Methods in Applied Mechanics and Engineering* 1982; **32**:199–259.
48. Hughes THR. *The Finite Element Method*: *Linear Static and Dynamic Finite Element Analysis*. Dover: New York, 2000; 562–564.
49. Heil M. An efficient solver for the fully coupled solution of large-displacement fluid–structure interaction problems. *Computer Methods in Applied Mechanics and Engineering* 2004; **193**:1–23.
50. Saad Y, Zhang J. Enhanced multi-level block ILU preconditioning strategies for general sparse linear systems. *Journal of Computational and Applied Mathematics* 2001; **130**:99–118.
51. Bathe KJ, Wilson EL. *Numerical Methods in Finite Element Analysis*. Prentice-Hall: Englewood Cliffs, NJ, 1976.
52. Jansen KE, Whiting CH, Hulbert GM. A generalized-α method for integrating the filtered Navier–Stokes equations with a stabilized finite element method. *Computer Methods in Applied Mechanics and Engineering* 2000; **190**:305–319.
53. Shu C, Wang L, Chew YT. Numerical computation of three-dimensional incompressible Navier–Stokes equations in primitive variable form by DQ method. *International Journal for Numerical Methods in Fluids* 2003; **43**: 345–368.

DOI: 10.1002/fld